SRESA's International Journal of

LIFE CYCLE RELIABILITY AND SAFETY ENGINEERING

Vol.4 **Issue No.3** **July–Sep. 2015** **ISSN – 2250 0820**

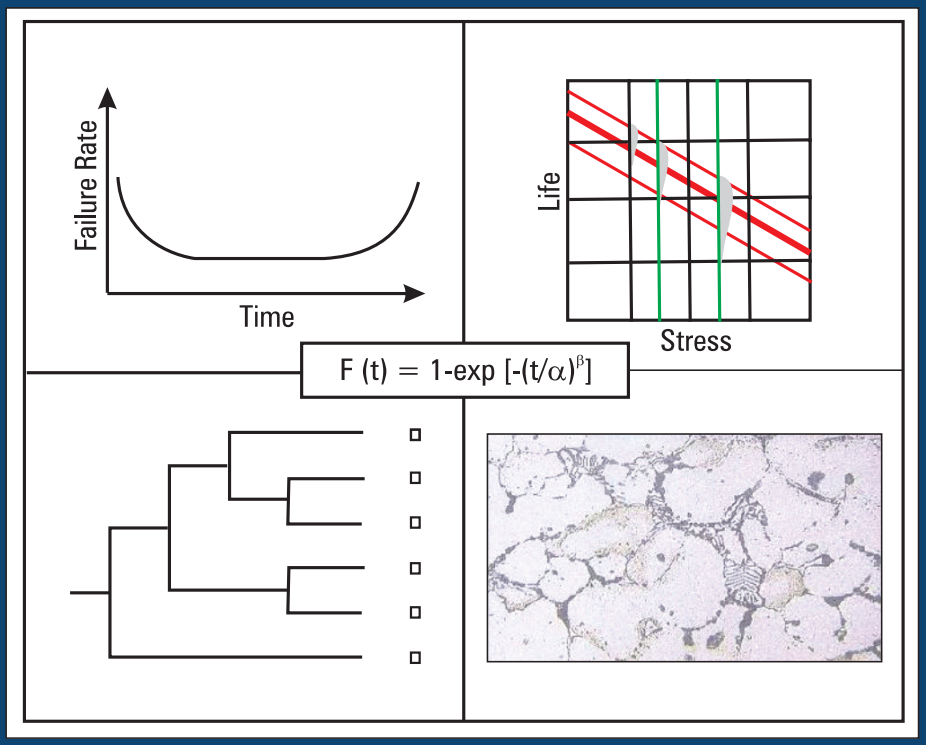

Chief-Editors

P.V. Varde
A.K. Verma
Michael G. Pecht

Society for Reliability and Safety

website: http://www.sresa.org.in

SRESA Journal of Life Cycle Reliability and Safety Engineering

Extensive work is being performed world over on assessment of Reliability and Safety for engineering systems in support of decisions. The increasing number of risk-based / risk-informed applications being developed world over is a testimony to the growth of this field. Here, along with probabilistic methods, deterministic methods including Physics-of-Failure based approach is playing an important role. The International Journal of Life Cycle Reliability and Safety Engineering provides a unique medium for researchers and academicians to contribute articles based on their R&D work, applied work and review work, in the area of Reliability, Safety and related fields. Articles based on technology development will also be published as Technical Notes. Review articles on Books published in the subject area of the journal will also form part of the publication.

Society for Reliability and Safety has been actively working for developing means and methods for improving system reliability. Publications of quarterly News Letters and this journal are some of the areas the society is vigorously pursuing for societal benefits. Manuscript in the subject areas can be communicated to the Chief Editors. Manuscript will be reviewed by the experts in the respective area of the work and comments will be communicated to the corresponding author. The reviewed final manuscript will be published and the author will be communicated the publication details. Instruction for preparing the manuscript has been given on inside page of the end cover page of each issue. The rights of publication rest with the Chief-Editors.

SCOPE OF JOURNAL

System Reliability analysis	**Structural Reliability**	**Risk-based applications**
Statistical tools and methods	Remaining life prediction	Technical specification optimization
Probabilistic Safety Assessment	Reliability based design	Risk-informed approach
Quantitative methods	Physics-of-Failure methods	Risk-based ISI
Human factor modeling	Probabilistic Fracture Mechanics	Risk-based maintenance
Common Cause Failure analysis	Passive system reliability	Risk-monitor
Life testing methods	Precursor event analysis	Prognostics & health management
Software reliability	Bayesian modeling	Severe accident management
Uncertainty modeling	Artificial intelligence in risk and reliability modeling	Risk-based Operator support systems
Dynamic reliability models	Design of Experiments	Role of risk-based approach in Regulatory reviews
Sensitivity analysis	Fuzzy approach in risk analysis	Advanced electronic systems reliability modeling
Decision support systems	Cognitive framework	Risk-informed asset management

SRESA AND ITS OBJECTIVES

a) To promote and develop the science of reliability and safety.

b) To encourage research in the area of reliability and safety engineering technology & allied fields.

c) To hold meetings for presentation and discussion of scientific and technical issues related to safety and reliability.

d) To evolve a unified standard code of practice in safety and reliability engineering for assurance of quality based professional engineering services.

e) To publish journals, books, reports and other information, alone or in collaboration with other organizations, and to disseminate information, knowledge and practice of ensuring quality services in the field of Reliability and Safety.

f) To organize reliability and safety engineering courses and / or services for any kind of energy systems like nuclear and thermal power plants, research reactors, other nuclear and radiation facilities, conventional process and chemical industries.

g) To co-operate with government agencies, educational institutions and research oganisations

SRESA's International Journal of

LIFE CYCLE RELIABILITY AND SAFETY ENGINEERING

Vol.4 Issue No.3 July–Sep 2015 ISSN – 2250 0820

Chief-Editors

P.V. Varde
A.K. Verma
Michael G. Pecht

SOCIETY FOR RELIABILITY AND SAFETY

Typeset & Printed

EBENEZER PRINTING HOUSE
Unit No. 5 & 11, 2nd Floor, Hind Services Industries,
Veer Savarkar Marg,
Dadar (west), Mumbai -28
Tel.: 2446 2632/ 3872
E-mail: outwork@gmail.com

Life Cycle Reliability and Safety Engineering
Vol.4 Issue 3 (2015) 01-08

Reactivity Initiated Transient Analysis of 2 MW Upgraded Apsara Reactor

Tej Singh, Tanay Mazumdar, Jainendra Kumar, P. V. Varde
Research Reactor Services Division, Bhabha Atomic Research Centre, Mumbai, 400085
Email: t_singh@barc.gov.in

Abstract

2 MW Upgraded Apsara reactor is an open pool type light water research reactor which has been proposed to be built in India. U_3Si_2-Al dispersion type low enriched uranium (LEU) (17.0 wt%) fuel will be used for this reactor. Expected maximum in-core thermal neutron flux is 6.1×10^{13} n/ cm^2/s. In order to ensure safe operation of the reactor, safety analysis has been carried out for a number of possible reactivity insertion events simulated in the reactor.

Keywords: Upgraded Apsara; Safety; Transient; LORI.

1. Introduction

Nuclear reactors are meant for safe and sustained production of energy from nuclear fission reaction. Hence, it is very important to study various safety aspects of reactors which help us to figure out whether reactors will remain safe or become vulnerable under any Postulated Initiating Events (PIEs). The term 'Postulated Initiating Event' refers to an unintended event including an operating error, equipment failure or external influence that directly or indirectly challenges basic safety functions of a reactor. Typically, such an event necessitates protective actions (automatic or manual) to prevent or mitigate undesired consequences to reactor equipment, reactor personnel, the public or the environment. Postulated initiating events are identified based on engineering evaluation, logical analysis and past operating experience. Listing of the initiating event as applicable to Upgraded Apsara Reactor has been done based on the guide lines given in IAEA safety standard series no. NS-R-4 (IAEA, 2005). The PIEs considered here are mainly responsible for reactivity insertion accidents (RIA) like reactor start up accident, loss of regulation incident (LORI) etc. In order to assess the severity of such accidents, we have already developed computer codes – RITAC (Mazumdar et al., 2012) and SACRIT (Singh et al., 2013) which solve point kinetics equation as well as thermal hydraulics equations in a coupled manner for plate type fuel geometry to analyze reactivity induced transients. In RIAs, positive reactivity insertion in a given manner makes neutron density and subsequently fuel, clad and coolant temperatures increasing with time and this rise in fuel and coolant temperature causes reactivity feedback which perturbs reactivity and ultimately the neutron density. This paper is written in following way. In section 2.0, Upgraded Apsara is briefly introduced. Then input data and underlying assumptions of the analysis are given in section 3.0. Modeling for RIA in computer codes and calculation of integral kinetics parameters are given in section 4.0 and 5.0 respectively. Subsequent sections are dedicated to steady state thermal hydraulic analysis followed by results of all PIEs, namely start up accident, LORI etc. Finally conclusion is drawn based on the analysis carried out.

2. 2 MW Upgraded Apsara Reactor

Upgraded Apsara Reactor is a 2 MW swimming pool type reactor. It uses Low Enriched Uranium (LEU) based U_3Si_2 fuel dispersed in Aluminum matrix (17 wt% U^{235} enrichment). The reactor core consists of 11 Standard Fuel Assemblies (SFAs) and 4 Control Fuel Assemblies (CFAs) as shown in Fig.1. A standard fuel assembly consists of 17 fuel bearing plates and two aluminum inert plates swaged into grooves provided in aluminum side plates. A water gap of 2.5 mm is maintained between two successive fuel/ inert plates. Each fuel plate has a meat thickness of 0.7 mm and the fuel meat is cladded with 0.4 mm thick aluminum sheet. Control fuel assembly is basically a standard fuel assembly except the fact that there are 12 fuel plates with a water gap of 2.4 mm between them. At either end of the assembly, 9.45 mm wide recess is provided for movement of fork type twin absorber blade. Out of four control fuel assemblies, two will work as Control cum Shutoff Rods (CSRs) and other two will work as Shut-Off Rods (SORs).

The reactor core is cooled by de-mineralized water flowing from top to bottom through the core. Primary coolant pumps draw water from pool outlet line at a rate of 4900 lpm and it is passed through a heat exchanger where heat is rejected to secondary coolant. Calculation of core physics parameters of the reactor is given in (Singh et al., 2013).

3. Input Data and Assumption

Based on steady state analysis it is found that 50% IN condition of the control blades is the most conservative for thermal hydraulic calculation. Hence, the same is considered for carrying out the transient analysis. Computer codes RITAC and SACRIT are used to carry out the transient calculation. Underlying assumptions of the analysis are given below.

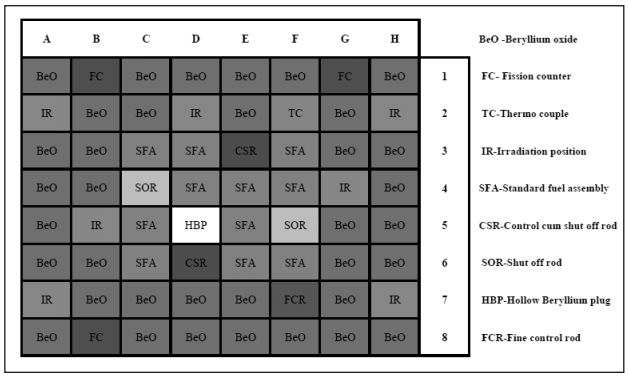

Fig.1: Equilibrium core configuration of upgraded Apsara

(i) Transients, caused due to uncontrolled addition of positive reactivity, lead to rise in reactor power. In normal operation scenario, this power surge is arrested by tripping the reactor on regulation/ protection parameters.

(ii) However, in the analysis, no credit has been given to regulation system trips. In addition to this, it is assumed that the first trip is ignored and the reactor is tripped on next available trip to assess the severity of the transients.

(iii) Reactor trip is manifested by dropping two control rods (partly inserted into the core) and two shut off rods (parked outside the core) into the core though in the analysis a typical combination of one control rod and one shut off rod, which adds least negative reactivity worth (~69 mk) amongst all the possible combinations of two out of four rods, has been considered to simulate the worst possible case.

(iv) The analysis has been performed considering maximum drop time of SORs and CSRs as 0.5 sec for 90% drop and 2.5 sec. for the 100% drop.

(v) A time delay, caused due to signal processing, before the rods fall into the core is taken to be about 500 ms in the calculation.

(vi) The reactivity feedback coefficients used in the calculation are (a) Doppler coefficient: Responsible for increased neutron absorption in U^{238} epithermal resonance regime as the temperature increases in fuel, (b) Water temperature coefficient: Responsible for hardening of neutron spectrum and (c) Water void/density coefficient: Responsible for neutron leakage due to change in water density as the water is heated up or boiled. Core averaged values of the reactivity feedback coefficients are considered for both average and hot channel.

(vii) Six group effective delayed neutron fraction (β_{eff}) are used in the calculation. Their values have been determined with the help of a computer code NEMSQR (Singh et al., 2014).

(viii) The nominal flow rates for control and standard fuel assemblies are taken to be 190 lpm and 240 lpm respectively. At 2 MW, maximum assembly power is 173 KW for SFA, 124 KW for CFA-CSR and 140 KW for CFA-SOR. Axial peaking factors for SFA, CFA-CSR and CFA-SOR are 1.36, 1.63 and 1.33 respectively while local peaking factors are 1.45, 1.18 and 1.3 respectively.

(ix) Coolant inlet temperature remains at 38^0C throughout the transient.

(x) In order to carry out conservative analysis incorporating the uncertainty in single phase heat transfer coefficient correlation, heat transfer coefficient value is taken 15% lesser than the value obtained from the correlation (Kristof and Vojtek, 2003).

4. Modeling for RIA in Computer Codes

As mentioned earlier, coupled system of equations of neutron kinetics and thermal hydraulics are solved for modeling of RIAs. Point kinetics equations is a set of time dependent coupled linear ordinary differential equations which is valid for small sized reactor. In RITAC, point kinetics equations are solved numerically by piecewise constant approximation (PCA) method (Kinard and Allen, 2004). In SACRIT, point kinetics equations are solved numerically by fourth order Runge Kutta method. Neutron density or reactor power, obtained after solving point kinetics equation, is fed into thermal hydraulics equations which are energy conservation equations for fuel and clad regions and mass, momentum and energy conservation equations for coolant region. Thermal

hydraulics equations are solved by finite difference method for which spatial discretization is done by dividing fuel, clad and coolant into a number of meshes both laterally and axially. In order to obtain temperatures at all lateral as well as axial meshes, calculation is performed at each and every axial height starting from fuel bottom to fuel top. Simulation is started from an equilibrium state of reactor. This analysis is assumed to be open loop since residence time of transient is expected to be too short to affect the inlet temperature. This is how steady state temperatures in all meshes are calculated and then supplied to transient temperature calculation. In coolant region, apart from energy conservation equation, mass and momentum conservation equations are solved. Coolant mass flux at different axial height is calculated by solving mass conservation equation while the pressure drop across the coolant channel is calculated by solving momentum conservation equation. Two-channel analysis, hottest channel for finding out maximum fuel, clad, coolant temperatures while an average powered channel for finding out average fuel, clad, coolant temperatures followed by calculation of fuel and coolant temperature feedback, is incorporated into the code. In order to analyze transients which lead to air bubble formation in liquid coolant, a homogeneous mixture of liquid and gas phase of coolant is considered. In the codes, it is possible to calculate void fraction of coolant which helps to further calculate void reactivity feedback. For the calculation of coefficient of heat transfer from clad to coolant in different boiling regimes, starting from single phase liquid to film boiling, a number of correlations, which are suitable for plate type fuelled reactor, are used.

When both bulk coolant temperature (T_c) and wall temperature (T_w) are below coolant saturation temperature (T_{sat}), coolant remains in single phase liquid regime. For this regime with forced convection, Dittus-Boelter correlation is used for turbulent flow (i.e. Reynolds number (Re)>10000). The correlation is given following.

$$h_{FC} = 0.023 \frac{K_l}{D_H} (Re)^{0.8} (Pr)^{0.4} \quad (1)$$

where K_l is thermal conductivity of coolant (W/m/K), D_H is hydraulic diametre (m), Re is Reynolds number of coolant = $(G_m D_H)/\mu_l$; G_m is coolant mass flux (Kg/m^2/sec), Pr is Prandtl number of coolant = $(C_{pl}\mu_l)/K_l$; C_{pl} is specific heat of coolant (J/Kg/K), μ_l and μ_w are coolant viscosity (Pa-s) evaluated at temperatures T_c (^{0}C) and T_w (^{0}C) respectively. K_l, Re and Pr are calculated at T_c. If the flow is laminar (i.e. Re<2100), Roshenow and Choi correlation is used. It is given below.

$$h_L = 4.0 \frac{K_l}{D_H} \quad (2)$$

Here also K_l is calculated at T_c. In the codes, both Eqn. (1) and (2) are evaluated and maximum between the two values i.e. $h=\max(h_{FC},h_L)$ is taken as single phase heat transfer coefficient. This is done in order to maintain continuity between two flow regimes.

Nucleate boiling starts in coolant when wall temperature exceeds saturation temperature of coolant and reaches onset of nucleate boiling temperature (T_{ONB}) which is estimated using Bergles and Rohsenow correlation as given by

$$T_{ONB} = T_{sat} + 0.556 \left(\frac{\Phi}{1082 p^{1.156}} \right)^{0.463 p^{0.0234}} \quad (3)$$

where Φ is heat flux (W/m^2) and p is coolant pressure (bar). Nucleate boiling is of two types; subcooled boiling and saturated boiling. When wall temperature exceeds T_{ONB}, but bulk coolant temperature remains below T_{sat}, then it is called subcooled boiling and when bulk coolant temperature reaches T_{sat}, then it is called saturated boiling. For both types of nucleate boiling, Chen correlation, as given below, is used.

$$\begin{aligned} q'' &= h(T_w - T_c) = h_{NB}(T_w - T_{sat}) + h_{FC}(T_w - T_c) \\ \Rightarrow h &= h_{NB} \frac{T_w - T_{sat}}{T_w - T_c} + h_{FC} \end{aligned} \quad (4)$$

This is the general form of correlation which reduces to $h=h_{NB}+h_{FC}$ in case of saturated boiling. Eqn. (4) includes h_{NB}, heat transfer coefficient due to nucleate boiling and h_{FC}, heat transfer coefficient due to forced convection. h_{FC} is calculated from a modified Dittus-Boelter correlation as given following.

$$h_{FC} = 0.023 \left(\frac{G_m (1-x) D_H}{\mu_l} \right)^{0.8} Pr^{0.4} \left(\frac{K_l}{D_H} \right) F \quad (5)$$

where G_m is coolant mass flux (Kg/m^2/sec), x is steam quality, D_H is hydraulic diametre (m), μ_l is coolant viscosity, Pr is Prandtl number and K_l is thermal conductivity of coolant (W/m/K). F, known as Reynolds number factor, is multiplied in above

equation to account for two phase flow. It is calculated from following relation.

$$X_{tt}^{-1} = \left(\frac{x}{1-x}\right)^{0.9}\left(\frac{\rho_g}{\rho_l}\right)^{0.5}\left(\frac{\mu_g}{\mu_l}\right)^{0.1}$$
$$F = \begin{cases} 1 & , X_{tt}^{-1} \le 0.1 \\ 2.34\left(X_{tt}^{-1} + 0.213\right)^{0.736} & , X_{tt}^{-1} > 0.1 \end{cases} \quad (6)$$

h_{NB} is based on Forster-Zuber equation with a suppression factor S and is given below.

$$h_{NB} = 0.00122\left[\frac{K_l^{0.79} C_{pl}^{0.45} D_l^{0.49}}{\sigma_l^{0.5}\mu_l^{0.29} h_{lg}^{0.24} D_g^{0.24}}\right]\Delta T_{sat}^{0.24}\Delta p^{0.75} S \quad (7)$$

K_l is thermal conductivity of coolant (W/m/K), C_{pl} is specific heat of coolant (J/Kg/K), D_l is coolant density (Kg/m^3), σ_l is surface tension of coolant (N/m), μ_l is dynamic viscosity of coolant (Pa-s), h_{lg} is latent heat of vaporization of coolant (J/Kg), D_g is steam density (Kg/m^3), $\Delta T_{sat}=T_w-T_{sat}$ and $\Delta p=p_{sat}(T_w)-p_{sat}(T_{sat})$ where $p_{sat}(T_w)$ and $p_{sat}(T_{sat})$ are saturation pressure (Pa) at wall temperature T_w(^{0}C) and coolant saturation temperature T_{sat}(^{0}C) respectively. S is calculated using following relation suggested by Thurgood .

$$Re_{TP} = 1.0\times10^{-4}\, Re\, F^{1.25}$$
$$S = \begin{cases} 1.0/\left(1.0 + 0.12\, Re^{1.14}\right), & Re_{TP} < 32.5 \\ 1.0/\left(1.0 + 0.42\, Re^{1.14}\right), & 32.5 \le Re_{TP} < 50.9 \\ 0.1 & , \quad Re_{TP} \ge 50.9 \end{cases} \quad (8)$$

where Re_{TP} is two phase Reynolds number which is calculated based on Reynolds number (Re) and Reynolds number factor (F). Nucleate boiling exists as long as heat flux from clad to coolant remains below critical heat flux (CHF).

In two phase coolant flow, void fraction and steam quality calculation is required in order to modify coolant mass flux, coolant density etc. which has an effect on the estimation of heat transfer coefficient. Void fraction (α) is defined as the volume fraction of steam in total volume of two phase (liquid-steam) mixture. Steam quality (x) is nothing but the mass fraction of steam in total mass of same mixture. So there is a close relationship between these two quantities.

$$x = \frac{1}{1+\left(\frac{1-\alpha}{\alpha}\right)\left(\frac{D_l}{D_g}\right)} \quad (9)$$

where D_l and D are density of liquid and steam respectively at coolant temperature T_c. In subcooled boiling, it is assumed that a fraction of heat from clad to coolant is consumed in vapour generation and since bulk coolant temperature is below saturation temperature, some vapour or air bubble collapse. With this assumption, mass conservation equation of steam is modified and is given below.

$$\frac{\partial}{\partial t}\left(\alpha D_g\right) + \frac{\partial}{\partial z}\left(xG_m\right) = \frac{F_s q''}{h_{lg} D_H} - \lambda_s D_g \alpha \quad (10)$$

where G_m is coolant mass flux, q" is heat flux from clad to coolant, h_{lg} is latent heat of vaporization of coolant, D_H is hydraulic diameter, F_s is the fraction of heat consumed in vapor production and is defined as following.

$$F_s = \frac{1}{1 + f_p \frac{H_l}{1-\eta}} \quad (12)$$

f_p is an adjustable factor and is set to 1.3, $H_l=(h_{sat}-h_l)/h_{lg}$; h_{sat} and h_l are liquid enthalpy at T_{sat} and T_c respectively, $\eta=(D_l-D_g)/D_l$. λ_s is bubble collapse frequency which is determined as following.

$$\lambda_s = c\lambda_0\phi H_l^2 \quad (12)$$

where c=0.005, $\lambda_0=(H_w^2)/(K_{sat}D_lC_{psat})$; H_w is single phase heat transfer coefficient as given in section 2.2.8.1, K_{sat} is thermal conductivity of coolant at T_{sat}, C_{psat} is specific heat of coolant at T_{sat}, $\varphi=[h_{lg}/\{C_{psat}(T_{ONB}-T_{sat})\}]^2$; T_{ONB} is onset of nucleate boiling temperature. In saturated boiling, heat from clad to coolant is consumed completely in vapor generation and air bubble does not collapse since bulk coolant temperature reaches T_{sat}.

Both RITAC and SACRIT codes are benchmarked against slow as well as fast transients in a 10 MWth pool type graphite reflected light water research reactor (IAEA-TECDOC-643, 1992).

5. Calculation of Integral Kinetics Parameters

For a given reactor, values of kinetics parameters i.e. delayed neutron fraction (βi) and generation time (Λ) are not same as mentioned in text book which are, in general, applicable for infinite system. Reactors in reality are finite in size which causes neutron leakage from core. Since, delayed neutrons are less energetic than prompt neutrons, they are less likely to leak out from the core and hence, they are more "effective"

in causing fission. This effectiveness depends on core geometry which varies from reactor to reactor. Therefore, we have to calculate the effective delayed neutron fraction (β_{eff}) and generation time for each reactor separately. NEMSQR, which is a Nodal Expansion Method based Neutron Diffusion Theory code for square geometry, is capable to calculate these kinetics parameters. For calculation of the parameters, steady state direct and adjoint flux diffusion equations are solved (Singh et al., 2014).

For 2 MW Upgraded Apsara, effective delayed neutron fraction is estimated to be 0.0074 which has been conservatively taken as 0.0071 considering the uncertainty in calculation. Generation time has been taken as 50 μsec.

Table-1: Steady state thermal hydraulic analysis for SFA, CFA-CSR and CFA-SOR

Parameters	SFA	CFA-CSR	CFA-SOR
Fuel centerline temperature	90.3	84.1	87.1
Fuel-clad interface temperature	89.1	82.9	85.8
Clad-coolant interface temperature	88.4	82.3	85.2
Coolant outlet temperature	58.5	53.4	57.1
ONBR	1.37	1.47	1.42

6. Results and Discussion

6.1 Steady state thermal hydraulic analysis

In order to carry out steady state thermal hydraulic analysis for standard (SFA) and control (CFA-CSR and CFA-SOR) fuel assemblies, radially fuel meat is divided into 10 meshes and clad into 3 meshes while axially entire fuel plate is divided into 10 axial meshes. Table-1 shows comparison of results between hottest SFA, CFA-CSR and CFA-SOR.

It is to be noted that plate power is maximum for CFA-SOR followed by SFA whereas coolant velocity for SFA is lesser as compared to CFA-SOR. As a combined effect, fuel centreline, fuel-clad interface, clad-coolant interface and coolant outlet temperatures are found to be maximum for SFA. These temperatures are 90.3^{0}C, 89.1^{0}C, 88.4^{0}C and 58.50C respectively. Onset of nucleate boiling ratio (ONBR), which is a ratio of maximum clad-coolant (or clad outer surface) temperature to onset of nucleate boiling temperature (T_{ONB}), is found to be minimum for SFA amongst all assemblies though its value (1.37) implies sufficient margin of maximum clad outer surface temperature from T_{ONB}.

In view of the fact that at any point of time during reactor operation, reactor power and coolant flow may mismatch, an analysis is carried out considering reactor operation at (i) 115% power and nominal flow, (ii) Nominal power and 85% flow and (iii) 115% power and 85% nominal flow. Case-(iii) is considered to be the most conservative steady state thermal hydraulic analysis which shows no melting of fuel/clad or boiling of coolant for the present reactor (Table-2).

Table-2: Steady state thermal hydraulic analysis for SFA, CFA-CSR and CFA-SOR (85% flow and 115% power)

Parameters	SFA	CFA-CSR	CFA-SOR
Fuel centerline temperature	105.1	97.4	101.0
Fuel-clad interface temperature	103.6	96.0	99.6
Clad-coolant interface temperature	102.9	95.2	98.9
Coolant outlet temperature	65.7	58.8	63.8
ONBR	1.18	1.28	1.23

6.2 Start up accident

In this accident analysis, it is postulated that due to circuit malfunction control rods are withdrawn continuously from its most sensitive position at a maximum rate of travel with reactor initially critical at 1 Watt. However, reactor power at critical level except first approach to criticality will remain more than 1 Watt due to buildup of photo-neutron source. Uncontrolled withdrawal of control rods during reactor startup leads to uncontrolled reactivity addition into the core. In the analysis, only one control rod withdrawal case is considered. Maximum rod withdrawal speed will be 1.5 mm/sec and the corresponding maximum reactivity insertion rate will be ~ 0.22 mk/sec. This uncontrolled withdrawal of control rod will be terminated as soon as reactor trip is registered. Though control rods are normally kept at partially IN condition, they are considered to be in fully OUT condition in the present analysis since the former is less severe than latter. It is found that maximum reactivity of 6.26 mk is inserted into the core and log rate reaches 224 %/sec. Reactor power is peaked at 3.89 MW and maximum fuel centerline,

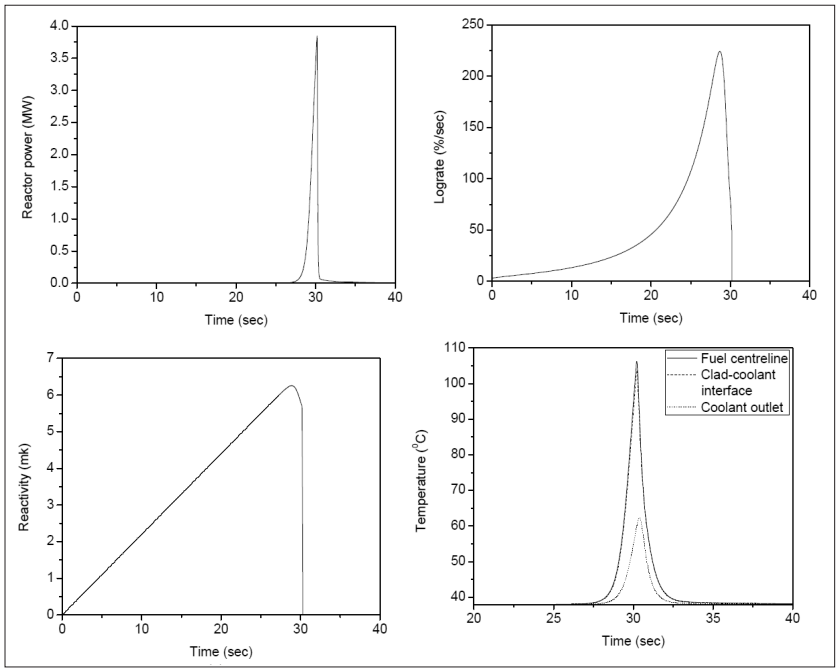

Fig.2: Results of start-up accident

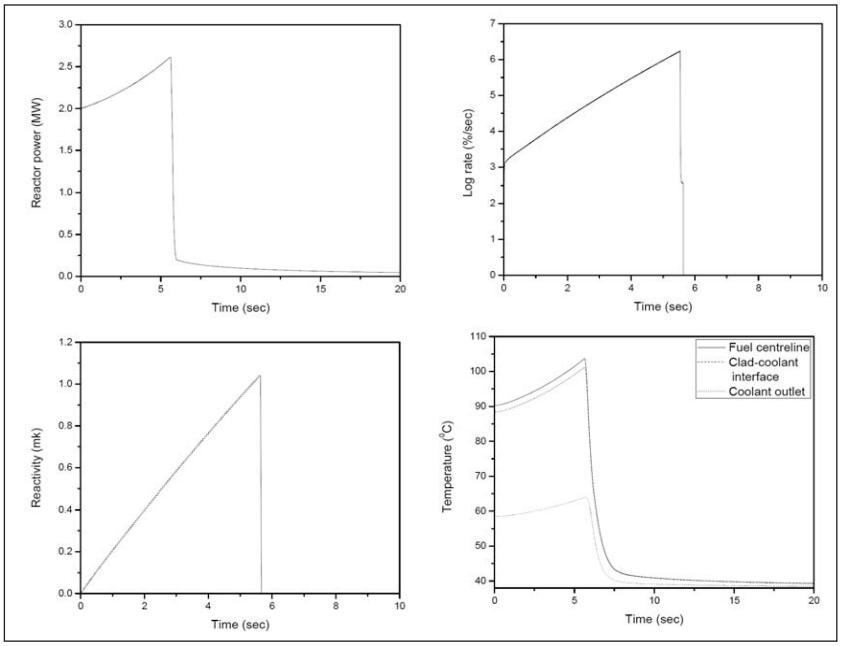

Fig.3: Results of Inadvertent withdrawal of CSR at full power operating condition

clad-coolant interface and coolant outlet temperatures of SFA are estimated to be about 113.9^{0}C, 111.0^{0}C and 65.8^{0}C respectively. Variation of reactor power, reactivity, lograte and fuel centreline, clad-coolant interface and coolant outlet temperature of SFA with time are given in Fig.2.

6.3 Inadvertent withdrawal of CSR at full power operating condition

In this accident analysis, it is postulated that during normal reactor operation at full power i.e. 2 MW with normal coolant flow through the core, one of the CSRs is withdrawn in uncontrolled manner with maximum permissible speed of 1.5 mm/sec. The corresponding maximum reactivity insertion rate will be ~ 0.22 mk/sec. In this analysis, first trip which is overpower trip at 2.3 MW, has been ignored and second trip, which is lograte at 6 %/sec, is taken into account. It is assumed that, uncontrolled withdrawal of control rod will be terminated as soon as the trip is registered. As a consequence, maximum reactivity of 1.04 mk is inserted into the core and log rate reaches up to 6.24 %/sec. During the transient, the peak power is reached upto at 2.61 MW and maximum fuel, clad and coolant temperatures of SFA are estimated to be about 103.7^{0}C, 101.2^{0}C and 64.0^{0}C, respectively. Variation of reactor power, reactivity, lograte and fuel centreline, clad-coolant interface and coolant outlet temperature of SFA with time are given in Fig.3.

6.4 Loss of regulation incident (LORI)

Reactivity control for start up and power regulation is achieved by controlled movement of fine control rod and control cum shut off rods in the reactor core. The fine control rod is used to adjust reactivity in smaller step on auto/manual mode while the control cum shut-off rods are meant for coarse adjustment of reactivity on manual mode. The regulating system employs three independent channels and works on 2/3 coincidence logic. The system design is such that a fault/defect beyond a pre-set level in any channel automatically leads to its rejection and the control action is taken over by the rest two channels without affecting reactor operation. Further malfunction in anyone of the remaining two channels before the rejected channel is rectified and restored would cause a reactor trip. In loss of regulation incident (LORI) analysis, enveloping scenario that positive reactivity getting added into the system at the maximum design rate by the way

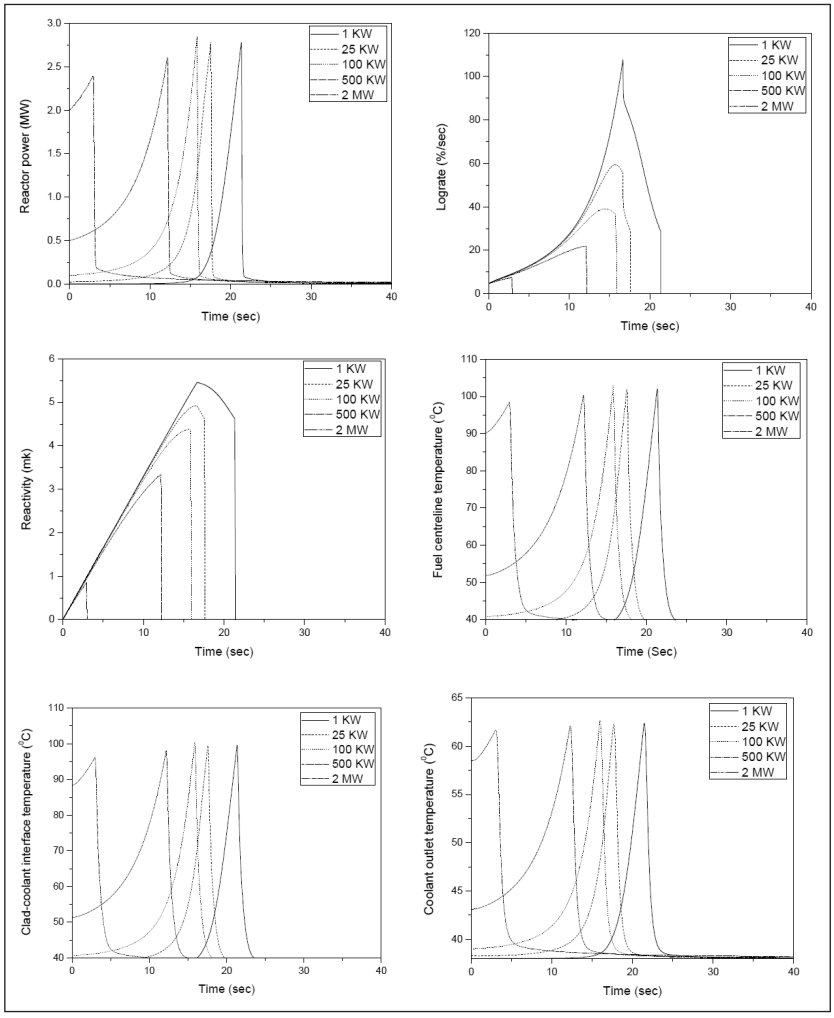

Fig.4: Results of LORI due to withdrawal of FCR alone

of continuous and uncontrolled withdrawal of (i) Fine Control Rod (FCR) alone and (ii) FCR and one of the CSRs together, are considered which in turn increases the reactor power.

6.4.1 Only FCR withdrawal case

The maximum withdrawal speed of FCR is limited to 16 mm/sec and the corresponding maximum addition of reactivity in the core is about 0.33 mk/sec. Reactivity worth of FCR is chosen to be less than the effective delayed neutron fraction (β_{eff}~7.1 mk) of the core to restrict the consequences of a loss of regulation scenario. Worth of the FCR in equilibrium core is about 5 mk. However, in the analysis, reactivity worth of the FCR has been conservatively assumed to be 10% higher than 5 mk considering the fact that the worth varies while the core evolves from fresh to equilibrium phase. In order to analyze the severity of reactivity initiated transients at different operating conditions, the transients are assumed to be initiated from five different initial power levels, namely 1 KW, 25 KW, 100 KW, 500 KW and 2 MW. Consequence of the transient initiated from 100 KW (or less) is more severe than those initiated from higher initial powers. This is expected because at higher initial powers the overpower trip level of 2.3 MW is reached earlier and thereby restricting further addition of positive reactivity. It is important to note that if credit is taken for the termination of the transients by the high log rate trip at 6% /sec instead of the overpower trip at 2.3 MW, the consequences of the LORI would be hardly of any concern.

Maximum reactivity inserted into the core is found to be about 5.46 mk and log rate reaches up to 108 %/sec. During the transient, the peak power is reached upto at 2.85 MW. Maximum fuel, clad and coolant temperatures are observed to be about 102.9^{0}C, 100.5^{0}C and 62.7^{0}C respectively for SFA. All the temperatures are well within their limiting value and no boiling occurred in the core.

Fig.4 show the variation of reactor power, reactivity, log rate and temperatures of fuel centreline, clad-coolant interface and coolant outlet with time for all above mentioned cases in SFA.

6.4.2 FCR and one of the CSRs withdrawal case

Withdrawal of FCR causes maximum reactivity addition at a rate of 0.33 mk/sec while withdrawal of one of the CSRs causes maximum reactivity addition at a rate of 0.22 mk/sec. If FCR and one CSR are inadvertently withdrawn together, which is considered to be extremely rare event, then positive reactivity will be added into the core at a rate of (0.33+0.22) = 0.55 mk/sec. Similar to analysis described in previous section, the transient is assumed to be initiated from five different initial power levels, namely 1 KW, 25 KW, 100 KW, 500 KW and 2 MW. Consequence of the transient initiated from 1 KW is more severe than those initiated from higher initial powers.

Maximum reactivity inserted into the core is found to be about 6.27 mk is and log rate reaches up to 237 %/sec. During the transient, the peak power is

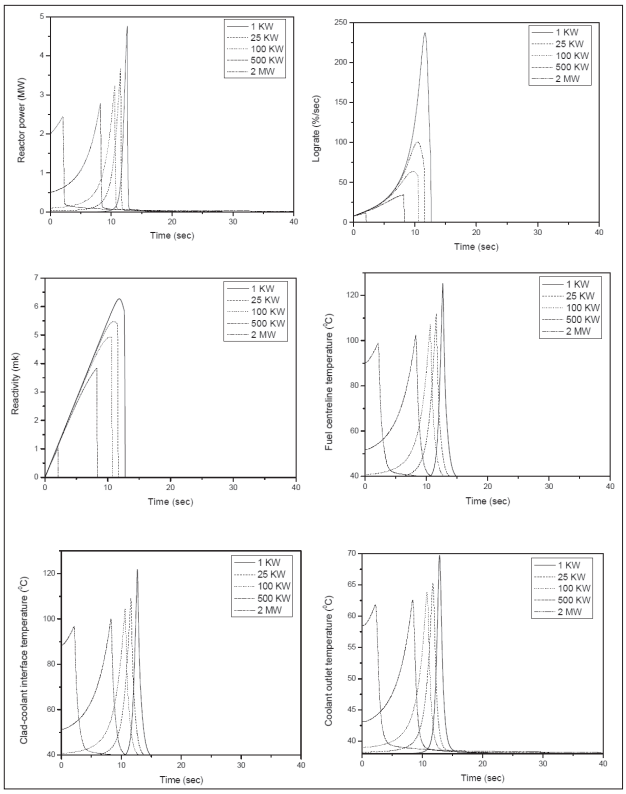

Fig.5: Results of LORI due to withdrawal of FCR and one of the CSRs

reached upto at 4.76 MW. Maximum fuel, clad and coolant temperatures are observed to be about 125.3^{0}C, 121.9^{0}C and 69.7^{0}C respectively for SFA. Though the bulk coolant temperature remains much below the saturation temperature (~115^{0}C), the clad-coolant interface temperature exceeds saturation temperature momentarily for about 0.18 sec.

Fig.5 show the variation of reactor power, reactivity, lograte and temperatures of fuel centreline, clad-coolant interface and coolant outlet with time for all above mentioned cases in SFA.

6.5 Removal of in-core experimental assembly

There is one position inside core where an experimental assembly can be loaded. Though this assembly will be removed from core only when the reactor is in shutdown state, a hypothetical scenario has been thought of where this assembly will be removed from a critical core of initial power 2 MW. In this analysis, reactivity load of the experimental assembly is restricted to be less than or equal to 2/3 of β_{eff} i.e. 5 mk which is added instantly into the core. As a consequence, peak power is reached upto at 6.64 MW. Maximum fuel, clad and coolant temperatures are observed to be about 133.9^{0}C, 128.8^{0}C and 84.8^{0}C respectively for SFA. Though the bulk coolant temperature remains much below the saturation temperature (~115^{0}C, in this case), the clad-coolant interface temperature exceeds saturation temperature momentarily for about 0.6 sec. Fig.15 shows the variation of reactor power, energy and temperatures of fuel centreline, clad-coolant interface and coolant outlet with time in SFA.

7. Conclusion

Analysis of various reactivity initiated transient events for 2 MW Upgraded Apsara reactor is carried out using two in-house computer codes - RITAC and SACRIT with a good degree of accuracy. Based on the detailed analysis, it is concluded that the core is safe under the reactivity initiated transient events postulated for the reactor. It is important to note that the maximum estimated clad temperature, 133.9^{0}C in the event of removal of in-core experimental assembly, is far below the melting point. In the same event, sub-cooled boiling of coolant takes place at the hot spot which has negligible effect due to its short duration (~0.6 sec).

Acknowledgement

We are thankful to Shri R.C. Sharma, Director Reactor Group and Shri S. Bhattacharya, Head RRDPD for their keen interest in this work. Thanks are due to all officers from RPNES, RRSD for their help and valuable suggestions.

References

1. IAEA-TECDOC-643, 1992. Research reactor core conversion guidebook, Volume 3: Analytical verification (Appendices G and H).
2. International Atomic Energy Agency, 2005. Safety of Research Reactors, IAEA Standard Series, Safety Requirements No. NS-R-4, Austria, Vienna.
3. Kinard, M., Allen, E. J., 2004. Efficient numerical solution of the point kinetics equations in nuclear reactor dynamics, Annals of Nuclear Energy, 31, 1039-1051.
4. Kristof, M., Vojtek, I., 2003. Uncertainty analyses for LB LOCA in VVER-440/213.
5. Mazumdar, T., Singh, T., Gupta, H. P., Singh, K., 2012. RITAC: reactivity initiated transient analysis code–an overview. Annals of Nuclear Energy, 43, 192-207.
6. Singh, T., Pandey, P., Mazumdar, T., Singh, K., Raina, V. K., 2013. Physics design of 2MW upgraded Apsara research reactor. Annals of Nuclear Energy, 60, 141-156.
7. Singh, T., Kumar, J., Mazumdar, T., Raina, V. K., 2013. Development of neutronics and thermal hydraulics coupled code–SAC-RIT for plate type fuel and its application to reactivity initiated transient analysis. Annals of Nuclear Energy, 62, 61-80.
8. Singh, T., Mazumdar, T., Pandey, P., 2014. NEMSQR: A 3-D multi group diffusion theory code based on nodal expansion method for square geometry. Annals of Nuclear Energy, 64, 230-243.

Life Cycle Reliability and Safety Engineering
Vol.4 Issue 3 (2015) 09-14

Reliability Enhancement of Furnace using Innovative Nontraditional Conical Electrode Shape Capacitors for Induction Furnace Power Management.

Prof. Avinash P. Paranjape[1], Dr. Ravindra M. Moharil[2]
[1]P.E.S. College of Engineering, Aurangabad, India, [2]Yashwantrao Chavan College of Engineering, Nagpur, India
E-mail: app1911@pescoe.ac.in

Abstract

This paper principally deals with the Reliable electrical power system requirements for induction furnace operation. The electrical aspect deals with the furnace power requirement to make it better and reliable functional by impedance parameters matching ($x_c = x_l$). This refers to the R, L, & C parameters of the system configuration; that sits between the source of high frequency power and the work coil; being used for heating. The paper states more particularly about reliable functioning of the capacitors having non-traditional conical electrode shapes. An induction furnace system has an active induction coil surrounding a crucible. A passive induction coil also surrounds the crucible. The source of ac current is provided to the active induction coil to produce a magnetic field that inductively heats and melts an electrically conductive material in the crucible. The passive induction coil is connected in parallel with a capacitor to form an L-C tank circuit. The resistance of the L-C tank circuit is reflected back into the circuit of the active induction coil to improve the overall efficiency of the induction furnace system. The tuning of a capacitor bank, using power electronics devices, develops a problem of harmonics injection in the system. This problem can be avoided by use of more secure and reliable capacitors having non-traditional conical electrode shapes, with supply system. The non-traditional conical shape electrode capacitors offer need base capacitance and current density combination, which enhance the operational Reliability, Life of the capacitor, and reduces puncturing of conductor foil in case of over currents.

Keywords: Secure and reliable tuning, Non-traditional Electrode shapes, Tuned circuit, Current sharing density, Elimination of capacitor banks, Reliability and performance life, Induction furnace.

1. Introduction

The use of induction furnaces for steel / metal ingot, making, has grown dramatically in the last decade throughout the world. The metal melting process involves the use of large quantities of energy, in a short time, and in some instances the process causes large decrease in the quality of electric power system, to electricity users, on the same network. The induction heating process basically consists in transmitting energy, by electromagnetic means, from a coil through which an alternative current is circulating. Induced currents in the conductive part, due to the well-known Foucault law, then heat the work piece; refer figure 1. [1]. Induction heating processes are mainly used either at low frequencies (around 30-60 Hz), usually in order to reach a temperature distribution as uniform as possible within the material before any forming process, or at much higher frequencies starting from the range of (100 Hz – 500 Hz) to maximum of (100 kHz– 1000kHz). [2]

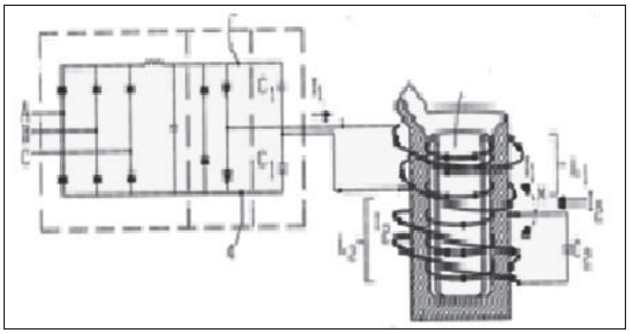

Figure.1- Induction furnace and its normal power circuit

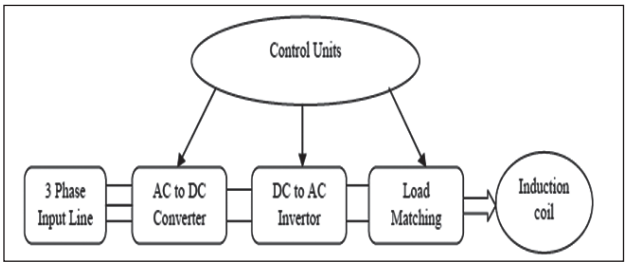

Figure.2 - The Standard supply system for induction furnace

Table: 1: Standard AVX make Capacitors and their ratings used for tuning with inductance of furnace

C (nF)	I rms Max. (A)	V rms Max. (V)	Q Max. kVARS	Rs (mΩ)	Rth (^{0}C/W)	L Max	H max
110	180	500	100	8x10-4x√F+0.19	0.86	55(2.165)	35(1.378)
210	300	500	150	8x10-4x√F+0.12	0.67	75(2.943)	40(1.575)
330	350	500	175	8x10-4x√F+0.15	0.54	75(2.943)	40(1.575)
510	500	500	250	8x10-4x√F+0.08	0.49	95(3.740)	45(1.772)
660	600	500	300	8x10-4x√F+0.06	0.38	95(3.740)	45(1.772)

C (nF)	I rms Max. (A)	V rmsMax. (V)	Q Max. kVARS	Rs (mΩ)	Rth (^{0}C/W)	L Max	H max
660	300	500	180	5x10-4x√F+0.25	0.6	75(2.953)	40(1.575)
1200	400	500	200	5x10-4x√F+0.20	0.56	75(2.953)	40(1.575)
2400	500	350	175	5x10-4x√F+0.17	0.55	75(2.953)	40(1.575)

C (nF)	I rms Max. (A)	V rmsMax. (V)	Q Max. kVARS	Rs (mΩ)	Rth (^{0}C/W)
4000	600	300	180	0.13	0.15
2400	500	400	200	0.15	0.20
1800	550	450	230	0.35	0.38
1200	500	500	200	0.20	0.22
660	450	500	220	0.26	0.32

Table – 2: Induction furnace powers and related frequencies

kW rating	Frequency
15-100	10 kHz
50-325	3 kHz
150-1500	1 kHz
350-3000	500 Hz
350-4000	100-200 Hz

The need of tuning the inductive coils with the capacitor banks is to create a secure and reliable resonant circuit, by making ($x_c = x_l$), to improve the power factor, and make it more and more close to unity. For this purpose, the capacitor banks are used, and fired using P.E. devices, at a particular time.

The work for this paper, and the study, in concern, carried out, is based on the world's most renowned (AVX) furnace power capacitor suppliers' data sheet records, and the practical needs, facing the problem of harmonic injection, because of firing of semiconductor devices in furnace power supplies. Usually for creating the resonance in the induction furnace power supply, most of the users deploy the capacitor banks, in shunt or series circuits; and fire the P.E. devices, to conduct the capacitor of approximately nearer to required value, to make a resonant circuit. This paper proposes to use the capacitor having non-traditional conical electrode shapes, which has a capability of providing secure and reliable, unseen parallel capacitor bank, which can offer the needed capacitance, without firing the P.E. (semiconductor) devices. This can eliminate the un-necessary generation of harmonics, caused by firing of P.E. devices. [3].

To carry out the exercise, the cone shaped electrode capacitor is chosen, having cone dimensions as, maximum radius 12.5 mm or 0.0125 m. Height of the cone is 50 mm or 0.05 m and slope length 51.54mm or 0.05154 m. The total cone area facing each other to form a capacitor is 0.001256004 m^2. The square root of this area value provides the dimensions of the equivalent parallel plates. The radius increment is differentiated in 90 equal parts; and as well the height. The cone surfaces are separated by 0.5 mm at their maximum radius side.

The capacitance 'C' is defined as C= εrε0 A / d. [3]

When a parallel plate capacitor which is considered as shown in figure-3, the total capacitance of the plate is a parallel combination of all individual differential capacitors developed between small unit height surface areas of the plate, can be found by the relation, capacitors in parallel, are added as a capacitance of parallel plates, being a sum of Σ Cunit = Σ ε * A unit / (unit distance of separation between parallel surface areas= 'd'). This distance of separation is normally used, is filled by the insulating dielectric material, like gaseous-air, SF6- or liquid – transformer oil- or

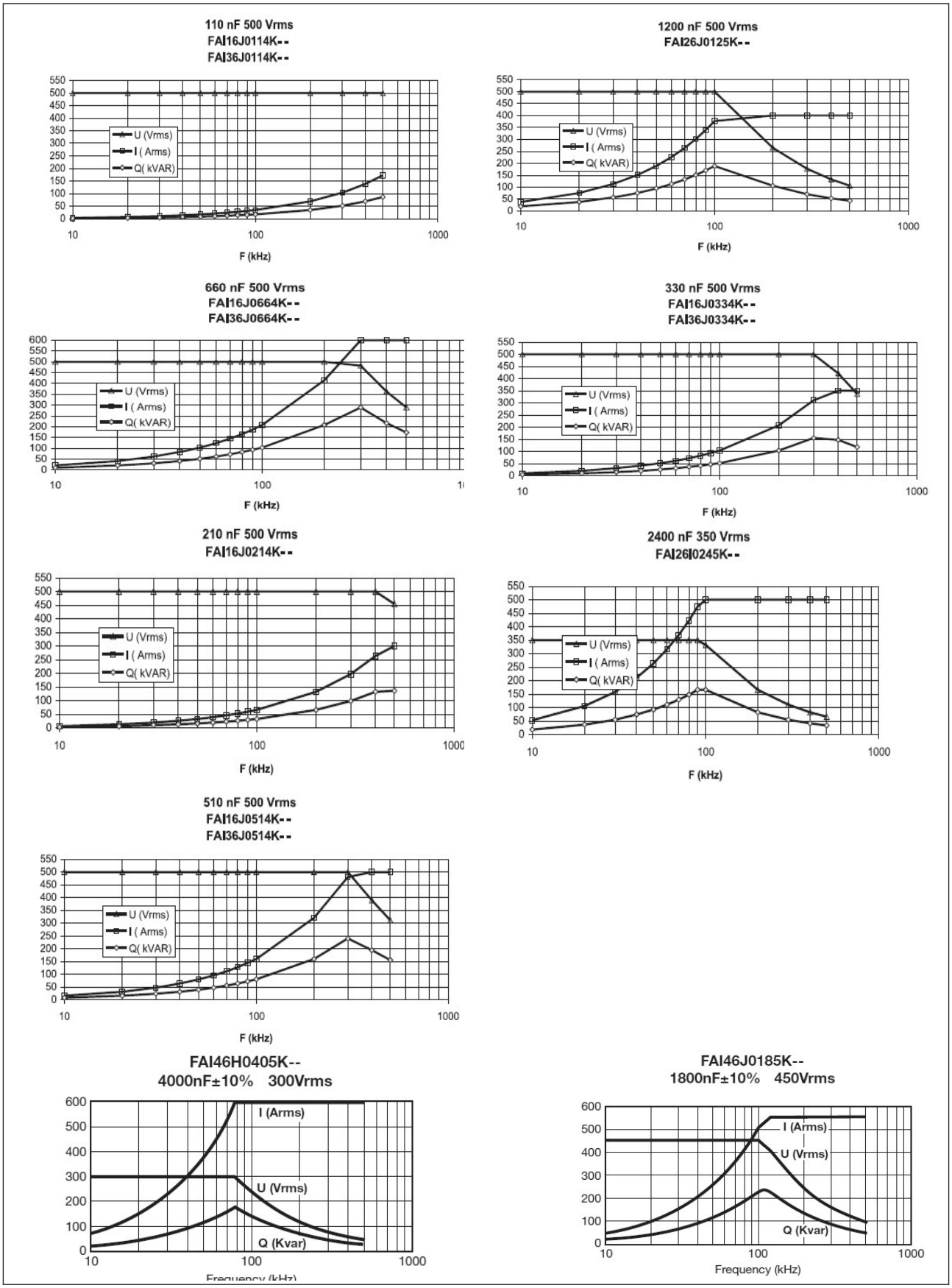

Figure- 3 Set of Graphs indicating Capacitors characteristics during TUNING and voltage built up: from data sheet of AVX corporation manual. [4]

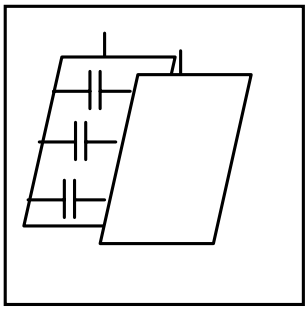

Figure.3 - Parallel plate capacitor

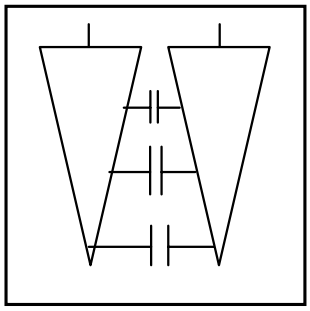

Figure.4 - Conical electrode capacitor

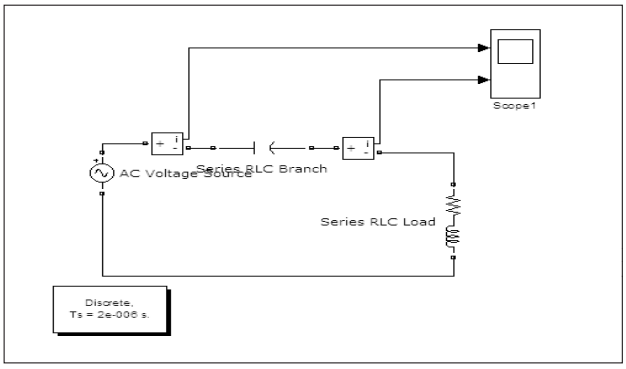

Figure-8 Parallel Capacitors by conical shape in series with Furnace

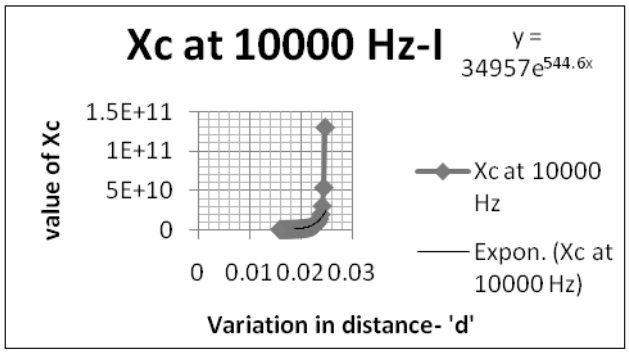

Figure. 5- Performance at frequency 10000 Hz. Broad Zone.

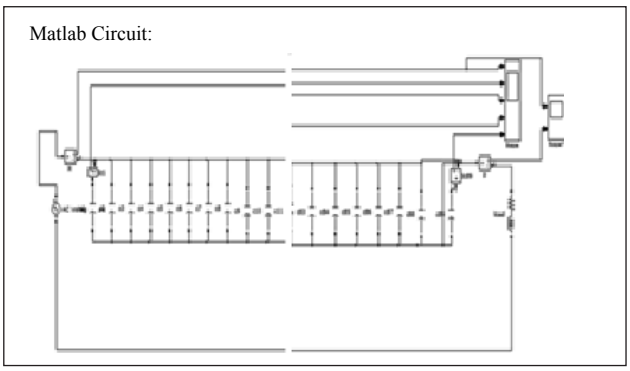

Figure- 9 Matlab Circuit

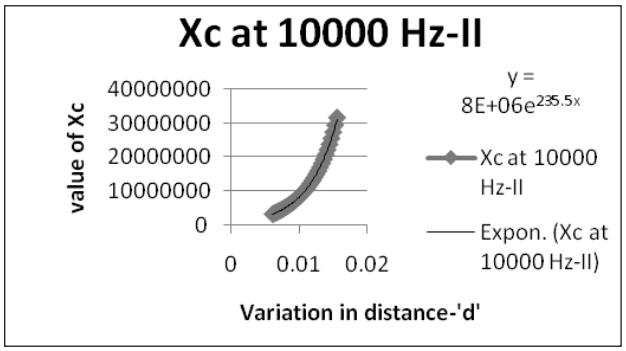

Figure.6- Performance at frequency 10000 Hz. Fine Zone

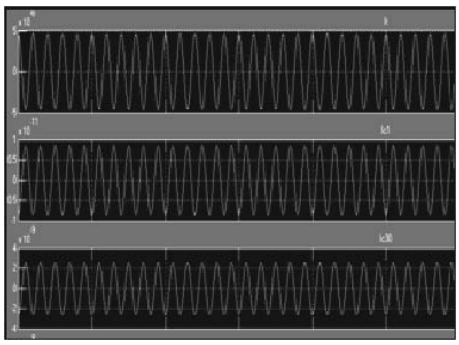

Figure-10 Wave forms of sample conical capacitors in series

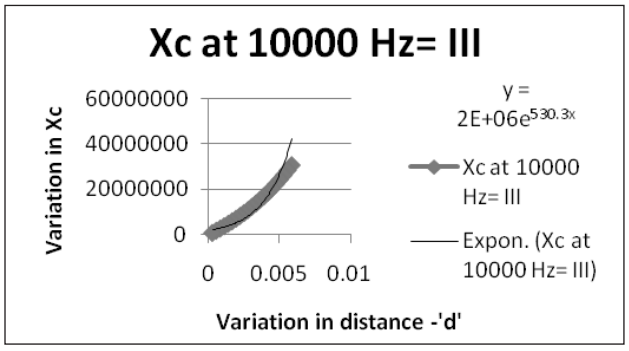

Figure -7 Performance at frequency 10000 Hz. More Precise zone.

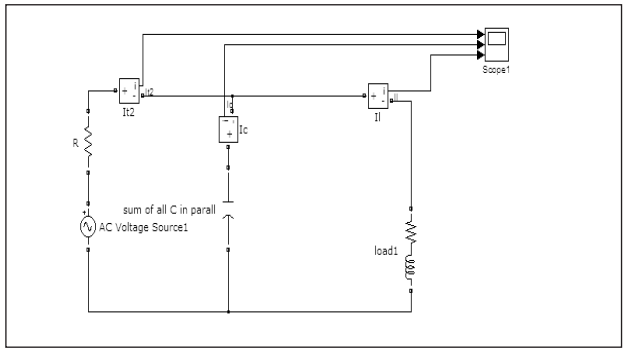

Figure-11 Parallel Capacitors by conical shape in parallel with Furnace

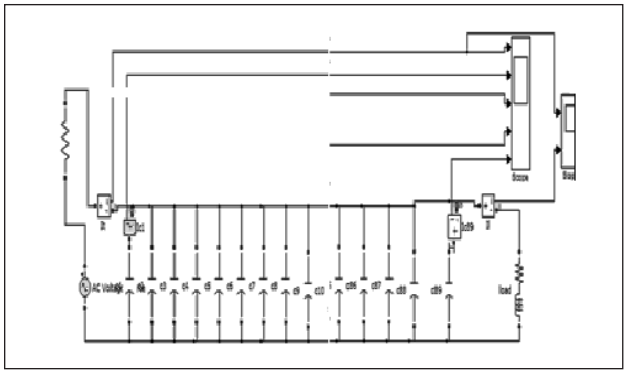

Figure-12 Matlab Circuit

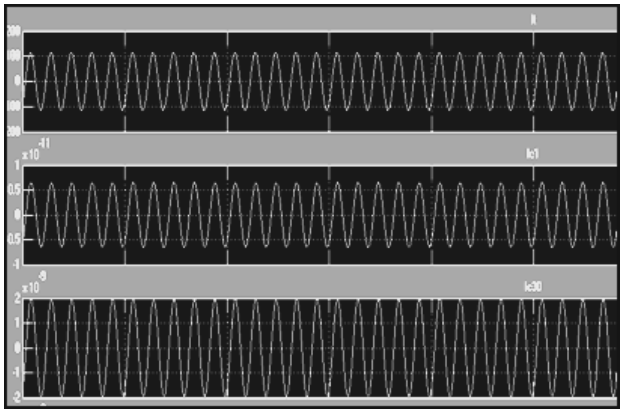

Figure-13 wave forms of sample conical capacitors in parallel

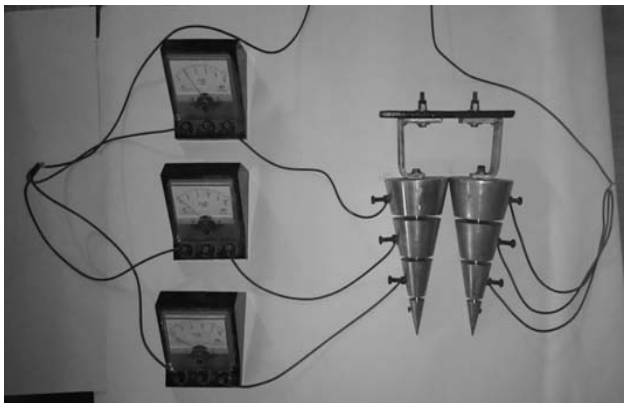

Figure-14 Capacitor's Arrangement for experimentation

solid- paper, mica and so on. The permittivity of that dielectric material is indicated as 'ε'. This ε- is a product of relative permittivity 'εr' and the absolute permittivity 'ε0'.

2. New Concept

Since all the unit height areas have same dimensions, same distance of separation, the value of each individual capacitor is same for all 'n' capacitors considered along the height. Hence total capacitance of the parallel plates is just = n* Cup.

Whereas application of same logic for the capacitor having non-traditional cone shape electrodes, the individual capacitance of conical shapes Cuc has different values for each one, figure-4. In such case the characteristics for conical shape types of capacitors are studied and the value of x_c, offered by that individual is plotted, for the frequency of 10000 Hz. For understanding the concept jist, and therefore the frequency chosen is neither the lower range frequency in the order of multiples of ten, like 50 Hz or 60 Hz, neither the high frequency range in more than 100 kHz. [5][6][7]

The plotted graphs shown, are representing the conical capacitor electrode shape model sectionalized in three parts of X_c values of the 90 divisions, as said in above description and are self explanatory, as well indicating the property of a conical shaped electrode capacitor, to offer the variable capacitive reactance x_c in one unit.

It shows the fact and a facility in one unit mass conical shaped electrode, to offer the variety of capacitor creating parameters, which are able to provide different areas of electrode face, different distance of separation of the areas, and different polarizability of a medium in a homogeneous condition to offer different permittivity, creating a different capacitor at each point on its surface. Whenever, at whatever frequency and where ever the supply frequency makes secure and reliable auto 'Tuning' with the inductive reactance of the inductance furnace, that portion of the cone making tuned capacitance, will offer the minimum impedance path, and share the major portion of load current. The current density for that electrode portion will be also less and develop less heat, in comparison with thin film gang capacitor. Hence it can reduce the capacitor puncturing problem; it does not require external switching firing, so it can prevent harmonics generation.

The basic concept behind this is the elimination of a capacitor bank having fixed capacitance, and needs to get fired as per need, at a particular time, required to be watched and having a step change in a capacitance.

When the non-traditional type electrode capacitors like a conical electrodes, are used, then that capacitor automatically provides the secure and reliable needed capacitance without firing, and without step change in a capacitance.

MATLAB simulation Model for series connected capacitor to Induction Furnace.

3. Experimentation

The experimentation was carried out on an induction furnace works on 3 kHz, and 10 Khz supply frequencies at M/S Chaitanya Electromagnets, Industrial Area MIDC Waluj Aurangabad [MS] India. The results obtained were as follows.

Table-3 Experimentation Results

10 kHz.	Xc at 10khz	Xc at 10 khz	Xc at 10 khz
Impedance	50090.28965	16231.54205	9689.21329
Mathematical	1A10= 0.0079	2A10= 0.024	3A10= 0.04
Actual	0.007	0.02	0.035
3kHz.	Xc at 3 khz	Xc at 3 khz	Xc at 3 khz
Impedance	166967.6322	54105.14018	32297.37763
Mathematical	1A3= 0.0023	2A3= 0.0073	3A3= 0.012
Actual	0.002	0.006	0.009
50Hz.	Xc at 50hz	Xc at 50 hz	Xc at 50 hz
Impedance	10018057.93	3246308.411	1937842.658
Mathematical	1A50= 39.9 mA	2A50= 123.21mA	3A50= 206.4 mA
Actual	35mA	114	198

4. Conclusion

The non conventional capacitor shapes are found offering the needed secure and reliable current sharing trend, which a normal capacitor bank offers, for a particular frequency, making resonance with the furnace inductor. The most advantage is, the non-conventional electrode shaped capacitors DO NOT offer the STEP changes in capacitor values, and neither have the STEP changes in the currents carried by them. This new concept arrangement can give the changes more smooth, secure and reliable, even in microns of the measure and hence these values are more reliable.

The non-conventional electrode shaped capacitor offers a significant area for the current passing, hence PUNCTURING of capacitors because of FILM type electrodes can be avoided. This new system does not require any water cooling hence SAVES energy required for cold water circulation.

Since failure of capacitor can get reduced, results in avoiding the accidents, increases the SAFETY and RELIABILITY of the system performance, and safety of the persons in nearby area.

References

1. Induction furnace with improved efficiency coil system US 6542535 B2
2. Nihar P. Bara International Journal of Emerging Science and Engineering (IJESE), ISSN:2319– 6378,Volume - 2, Issue - 5,March 2014 80 Published By:Blue Eyes Intelligence Engineering & Sciences Publication Pvt. Ltd.
3. Data book, Northeast Power Systems, Inc. -Harmonic Filter & Power Capacitor Bank Application Studies
4. Electric Melting Furnace - A Review Sneha P. Gadpayle , Rashmi N. Baxi
5. AVX Corporation A Leading Worldwide Manufacturer and Supplier of Electronic Components

Life Cycle Reliability and Safety Engineering
Vol.4 Issue 3 (2015) 15-24

Assessment of Insulation Degradation of I&C Cables from Chemical and Mechanical Measurements

T. V. Santhosh[1], A. K. Ghosh[2] and B. G. Fernandes[3]
[1]Reactor Safety Division, Bhabha Atomic Research Centre, India, [2]Raja Ramanna Fellow, Department of Atomic Energy, India, [3]Department of Electrical Engineering, Indian Institute of Technology Bombay, India
E-mail: santutv@barc.gov.in

Abstract

Instrumentation and control (I&C) cables used in nuclear power plants (NPPs) are exposed to various deteriorative environmental effects during their operational lifetime. The factors consisting of long-term irradiation (at rather low dose rates, in the presence of oxygen), and enhanced temperature eventually result in insulation degradation. Monitoring of the actual state of the cable insulation and the prediction of their residual service life consist of the measurement of the properties that are directly proportional to the functionality of the cables (usually the elongation at break is used as the critical parameter). In view of this, accelerated thermal and radiation ageing of I&C cable insulation materials have been carried out and the degradation due to thermal and radiation ageing has been assessed using oxidation induction time (OIT) and oxidation induction temperature (OITp) measurements by differential scanning calorimetry (DSC). As elongation at break (EAB) is considered to be a benchmark characterization technique for polymeric materials, tensile tests have also been carried out on these cable materials to measure EAB for correlating with DSC findings. The scanning electron microscopy (SEM) performed on fresh and aged samples support relatively good correlation between chemical and mechanical properties.

Keywords: *Ageing, lifetime prediction, oxidation induction time, oxidation induction temperature, elongation at break, scanning electron microscopy, nuclear power plants.*

1. Introduction

As electrical cables are one of the long life items that have not been considered for replacement during the design life of NPPs, typically 40 years, assessing their degradation state and predicting remaining lifetime are very critical issues. The prediction of long-term ageing performance has been practiced for years by accelerated ageing tests; however, the relationship between artificial and natural aging is still under discussion. The use of accelerated thermal ageing based on the Arrhenius theory has many limitations and the effect of dose-rate on accelerated radiation ageing has been examined extensively [1][2]. Researchers have faced the challenge of simulating the environmental and operational conditions of low-voltage cables located inside and outside the containment and predicting the degradation processes caused by these stressors. The challenge is even more difficult considering that each cable manufacturer uses proprietary formulations, including many additives (antioxidants, flame retardants, dyes, fillers, curing agents, plasticizers and other chemicals for thermal and radiation stability) to the base polymer. Additives strongly affect the ageing characteristics of insulation or jacket compounds. Furthermore, geometry and design of the cables, as well as the fabrication procedures, can affect the overall ageing characteristics. Lastly, synergistic effects due to combined radiation and thermal ageing have complicated the understanding of this topic even further [3][4].

A nuclear power plant uses a large number of low voltage cables from various manufacturers for I&C applications. Although, all the manufacturers meet the required specifications there can be a significant variation in the performance of cables from manufacturer to manufacturer. This can be due to many factors such as design, material processing, purity of the raw materials, workmanship, etc. Also, a few manufacturers add plasticizers and other additives for enhanced performance and ease of manufacturing. The condition monitoring (CM) techniques such as insulation resistance testing, tensile elongation, differential scanning calorimetry, Fourier transform infrared spectroscopy, etc. will provide strong basis on the adequate performance of these cables. Ideally, condition monitoring data and trends

in cable performance indicators can guide the cable engineer's decisions to effectively manage the ageing and degradation in electrical cables, cable splices, or other accessories in a cable system before they reach the end of life or degraded performance that may adversely affect the safe and reliable operation of the associated components and systems [5][7].

In this paper, accelerated thermal and radiation ageing of polyvinyl chloride (PVC) based cable insulation materials have been carried out, and the thermal and radiation stability of these materials have been analyzed using differential scanning calorimetry (DSC) and tensile testing experiments. The exact onset exothermic peak could not be established from the thermograms obtained from the OIT measurement for these samples even after 8 hours of testing in the range from 180^{0}C to 220^{0}C. However, these samples have shown a good oxidation peak under OITp measurement. Alternatively, OITs were predicted from the approach developed by Gimzewski based on fundamental thermodynamic principles of DSC [8]. It was found from the experimental evaluations that the OIT fits an exponential function of EAB for both thermal and radiation ageing of insulation material. The scanning electron microscopy was performed on fresh and aged samples to assess the degradation and to correlate the DSC findings with EAB for remaining life assessment applications.

2. Ageing

Ageing is the continuous time-dependent degradation of materials due to service conditions, which include normal operation as well as transient conditions. The polymer materials used for the insulation and jacket materials in electric cables, cable splices, and terminations are susceptible to ageing and degradation mechanisms caused by exposure to many of the stressors encountered in NPP service conditions. The dominant stressors are temperature, radiation and the presence of oxygen for the majority of reactor systems. It should be emphasized that real service conditions usually involve synergistic effects between two or more of these stressors. In particular, dose rate effects can be a major factor in the degradation of cables in plants. In many polymers the dose required to reach a specific level of degradation is significantly lower when the dose is applied at low dose rates[2]. Polymer degradation is the result of two main causes. The first is the chemical degradation due to changes in the chemical structure of the polymer sample. The second cause of degradation is associated with physical changes in the polymer [10-12]. The main chemical ageing mechanisms are:

1. Scission of macromolecular chains, when two shorter chains are created by the breaking up of one. It is usually a scission of alkoxy or peroxide radicals. The effect is usually a mechanical weakening of the polymer.
2. Cross-linking reactions, this corresponds to the formation of a covalent link of two adjacent macromolecules. The increment of crosslink density forms a three dimensional network. With the increase of the density of those bonds, material stiffness usually increases too. Prolonged cross-linking causes embrittlement.
3. Oxidation, this leads to a modification and functionalization of the polymer chains. At the same time thermal oxidation is accompanied by the destruction of bonds in the macromolecules and influences the destructive processes.

For many of the polymers of interest in cables, oxidation is the dominant ageing mechanism and is initiated both thermally and by irradiation. In PVC, the loss of plasticizer from thermal ageing is also an important degradation mechanism. These mechanisms can result in embrittlement of the cable materials, increasing the probability of cracking of the insulation under mechanical stresses. The effect will manifest as reduced EAB. Such stresses can arise in the plant from handling, vibration, thermal cycling or from the way in which the cable is routed. In practice it is this loss of mechanical integrity which is the prime cause of failure of low voltage cable, resulting in the loss of electrical integrity.

The accelerated ageing tests are, generally, carried out on cable insulation materials to predict their life expectancy under service conditions. Ideally, an ageing test should subject the cable insulating material to typical electrical, mechanical and thermal stresses that are encountered in service. However, conducting life tests under normal operating conditions results in unacceptably long testing times. The most effective means to carry out accelerated ageing is by subjecting cable to enhanced stresses applied at higher than the normal operating values [9]. The difficulty with accelerated ageing tests is relating the life under high stress to the life under operating conditions. Since there is no well-established theoretical model to convert accelerated ageing test results to the life at operating stress, statistical regression techniques are used to develop empirical models that relate stress levels to insulation life [13].

3. Experimental

Experimental techniques can provide the means for evaluating the level of ageing and degradation of electrical cable insulation materials. Condition monitoring for electric cable systems involves inspection and measurement of one or more indicators, which can be correlated to the condition or functional performance of the electrical cable on which it is applied [14-15]. Furthermore, it is desirable to link the measured indicators such as elongationatbreak (EAB), insulation resistance (IR), etc. with an independent parameter, such as time or cycles, in order to identify trends in the condition of the cable [16-17].

A. Accelerated Radiation Ageing

1) *Samples:* The cables chosen for experiments are of low voltage type (≤ 1100V) as they are extensively being used in nuclear power plant I&C applications. The specifications of the cable chosen for radiation ageing experiments are shown in Table 1.

Table-1 Specifications of Cable for Radiation Ageing

Cable type	Specifications	Polymer type	
		Insulation	Sheath
Control cable	10 core, 1.5sq.mm, 650/1100V	PVC	PVC

Accelerated radiation ageing was carried out as per IEC 544 standard [18] under aerated condition in a gamma chamber having ^{60}Co gamma source at a dose rate of 0.17MRad/Hr. Experiment was carried out at room temperature covering the doses from 2.5MRad to 50MRad to simulate the radioactivity release during normal and accidental conditions of NPP.

2) *Measurement of OIT and OITp:* The OIT measurements were carried out using SETARAM DSC131 Differential scanning calorimetry in accordance with ASTM D3895-07 standard [19] in the range from 180^{0}C to 220^{0}C, and up to 8 hours on fresh and irradiated PVC cable insulation materials. However, none of the DSC heat flow signals indicated an exact onset oxidation point (exothermic peak) under isothermal condition for these samples. Therefore, an alternative method of obtaining the OIT is through OITp measurement. In this test, instead of maintaining a constant test temperature and measuring the time at which oxidation initiates, the temperature of the sample is increased at a constant specified rate (e.g., 10^{o}C/ min) in flowing oxygen and the temperature at which oxidation initiates is recorded, which is the OITp. The OITp measurements were carried out on fresh and irradiated samples of upto 50MRad dose conditions.

3) *Determination of OIT from Experimental OITp:* The theoretical model presented here is the one developed by Gimzewski [8]. The model combines oxidative degradation kinetics with fundamental thermodynamic principles used in differential scanning calorimetry. The primary thermally induced oxidation reaction that occurs in the DSC is given by:

$$RH + O_2 \rightarrow R\cdot + HO_2\cdot \quad (1)$$

where RH is an undamaged polymer chain, is a polymer free-radical, and is a hydroperoxide free-radical. Polymer free-radicals can be produced when energy is imparted to the molecule (for example, by ionizing radiation or elevated thermal exposure) that results in the ejection of an electron. In the absence of antioxidants these free radicals propagate the degradation of the polymer. Antioxidants react preferentially with the free radicals to form inert molecules, thus deterring the degradation of the polymer.

Assuming that the reaction in Eq. (1) follows an Arrhenius relationship, as was assumed by Gimzewski[8]. The corresponding rate equation for reaction (1) is:

$$\frac{d}{dt}[RH] = -[RH][O_2]Ae^{-\frac{E_a}{kT}} \quad (2)$$

Where A is a constant related to the initial polymer concentration, E_a is the activation energy, k is Boltzmann's constant, and T is the test temperature.

Direct measurement of the OIT is done in the isothermal mode of the DSC which is known as time-scanning method. In this mode, letting T = T_{iso}, Eq. (2) can be integrated until the antioxidant is exhausted to give the following:

$$\int \frac{d[RH]}{[RH][O_2]A} = -\int_0^{OIT} e^{-\frac{E_a}{kT}} dt = -(OIT)e^{-\frac{E_a}{kT_{iso}}} \quad (3)$$

Although OIT cannot be solved from this equation, this result will be used in the second method for determining OIT as described below.

Alternatively, the DSC can be operated in the temperature scanning mode. This provides a measure of the oxidation induction temperature

(OIT_p), which is the temperature at which the antioxidant is entirely consumed. In this mode the temperature of the polymer sample is raised at a constant rate until the antioxidant is exhausted, i.e., until the oxidation induction temperature is reached. The temperature ramp rate, dT/dt, can be introduced into Eq. (2) as follows:

$$\frac{d}{dT}[RH]\left(\frac{dT}{dt}\right) = -[RH][O_2]Ae^{-\frac{E_a}{kT}} \quad (4)$$

Integration of Eq. (4) from the initial temperature, T_0 to OITp and denoting the ramp rate by α gives:

$$\int \frac{d[RH]}{[RH][O_2]A} = -\frac{1}{\alpha}\int_{T_0}^{OIT_p} e^{-\frac{E_a}{kT}}\,dt \quad (5)$$

The integrals on the LHS of Eq. (3) and (5) are equal because both are integrated until the antioxidant is exhausted.

Therefore the RHS of Eq. (3) and (5) can be set equal. This gives for OIT:

$$OIT = \frac{1}{\alpha} e^{\frac{E_a}{kT_{iso}}} \int_{T_0}^{OIT_p} e^{-\frac{E_a}{kT}}\,dt \quad (6)$$

Thus, by measuring OIT_p and E_a, the integral in Eq. (6) can be evaluated numerically. Equation (6) provides the basis for a comparison between the OIT measured directly and the OIT calculated from the measured thermal parameters, OIT_p and E_a.

From the OITp measurement, activation energy of 1.38eV was considered for both insulation and sheath for OIT calculations. The plots of calculated OIT corresponding to the observed OITp with respect to radiation dose for insulation and sheath are shown in Figure 1 and Figure 2 respectively.

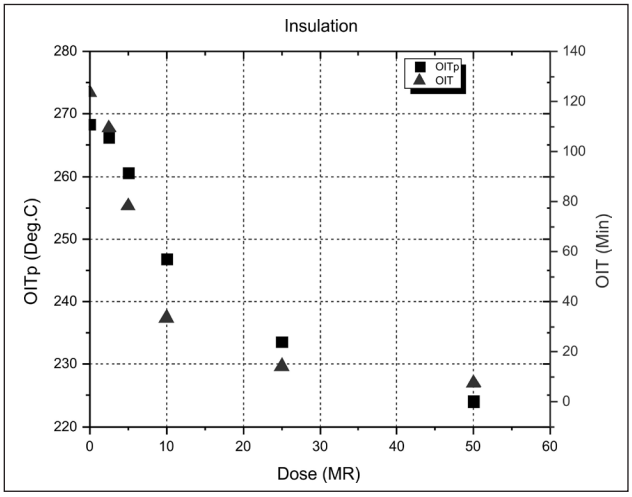

Figure-1 OIT vs. dose for insulation

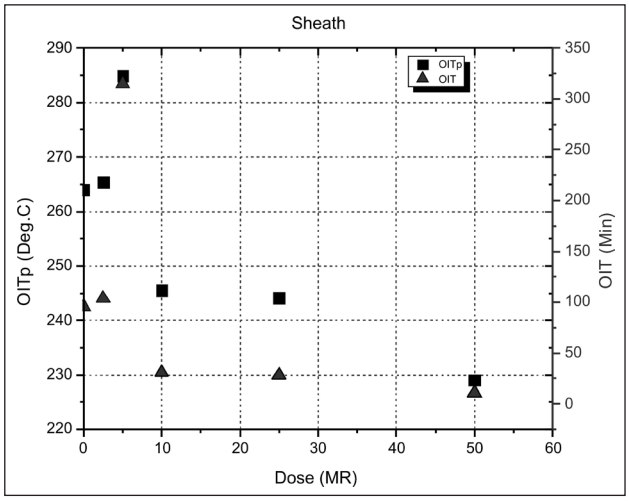

Figure-2 OIT vs. dose for sheath

4) *Measurement of EAB:* Tensile tests were performed using Tinius Olsen Universal Testing Machine with a load cell of 10kN in accordance with ASTM Standard D638 [20]. The tests were performed with an initial jaw separation of 25mm at a strain rate of 25mm/min. The data obtained under tensile testing was analyzed to determine the ageing process in the insulation and sheath material for degradation assessment. The plots obtained from the data analysis for insulation and sheath materials are shown in Figure 3 and Figure 4 with coefficient of determination being 0.439 and 0.976 respectively.

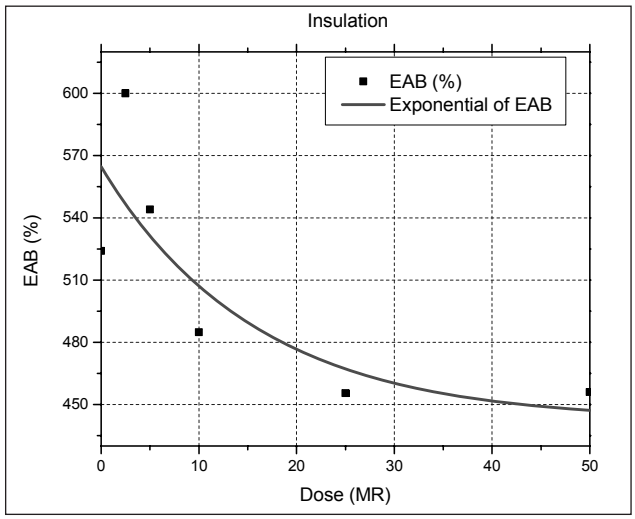

Figure-3 Exponential fit of EAB for insulation

It can be seen from Figure 3and Figure 4 that though the ageing process is exponential, the rates of degradation in the insulation and sheath

are significantly different. The empirical model obtained from the data analysis for insulation and sheath materials is:

$$EAB = A + Be^{-Cd} \quad (7)$$

Where, A, B and C are model parameters and d is the applied radiation dose. The parameter values and the standard error obtained from the data analysis for insulation and sheath are shown in Tables 2 and Table 3 respectively.

Table-2 Model Parameters for Insulation

Parameter	Value	Standard error
A	441.92	58.01
B	122.84	57.45
C	0.063	0.085

Table-3 Model Parameters for Sheath

Parameter	Value	Standard error
A	226.41	17.13
B	214.50	16.92
C	0.062	0.014

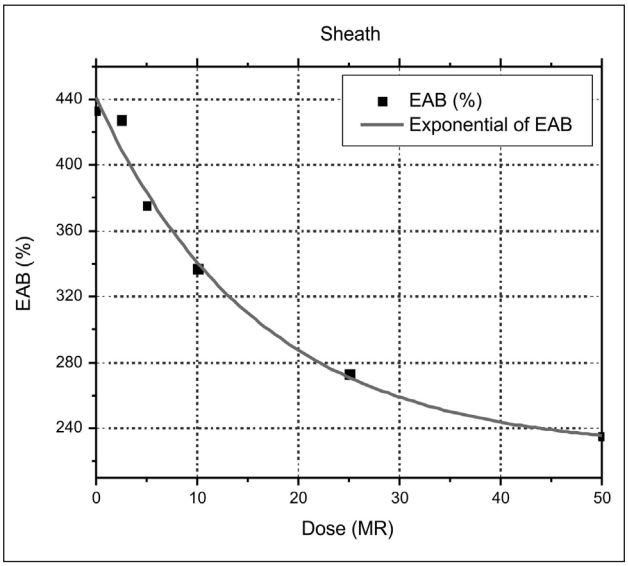

Figure-4 Exponential fit of EAB for sheath

5) *Correlation between OIT and EAB:* Since elongation is considered to be a benchmark characterization technique for polymers materials, the OIT obtained from DSC need to be correlated with EAB for degradation assessment and remaining life estimation applications. The exponential fit of OIT with coefficient of determination being 0.99 for insulation material is shown in Figure 5 and that of sheath material with coefficient of determination being 0.92 is shown in Figure 6.

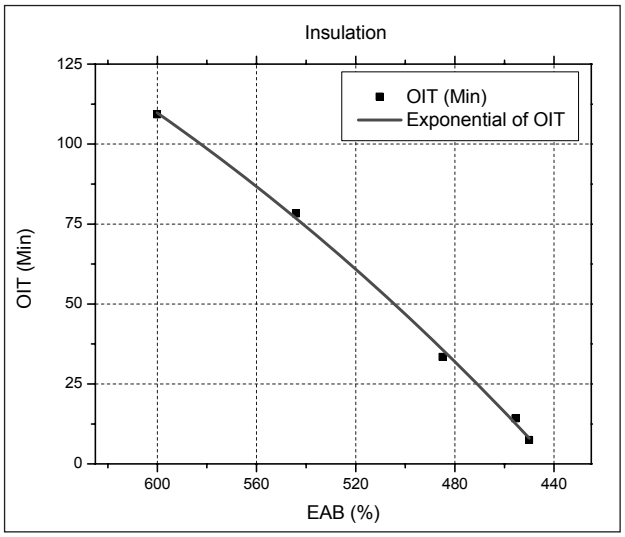

Figure-5 Exponential fit of OIT for insulation

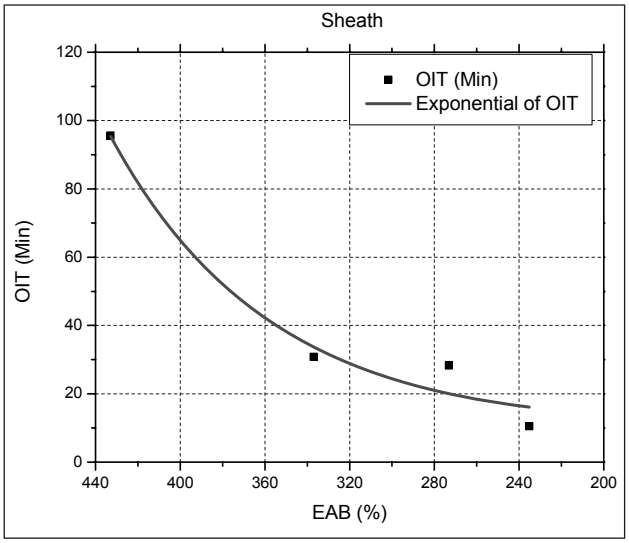

Figure-6: Exponential fit of OIT for sheath

It can be seen from Figure-5 and Figure-6 that though the relationship between EAB and OIT in both insulation and sheath follows exponential under radiation ageing, their rates of degradation is relatively different which was also evident from the tensile testing. This variation is due to the presence of various additives and plasticizers in the two materials used for enhancing the physical and mechanical properties. It is also evident that the thermo-oxidative stability of insulation is less compared to sheath at elevated dose levels.

B. Accelerated Thermal Ageing

1) *Samples:* The specifications of cable chosen for thermal ageing are shown in Table-4.

Table-4 Cable Specimen for Thermal Ageing

Cable type	Specifications	Polymer type	
		Insulation	Sheath
Signal cable	37 core, 1.5sq.mm, 1100V	FRLS PVC	HRPVC

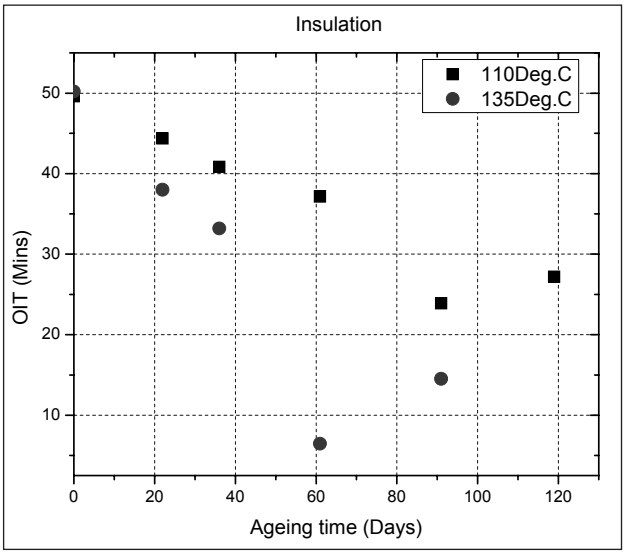

Figure-8 OIT vs. ageing time

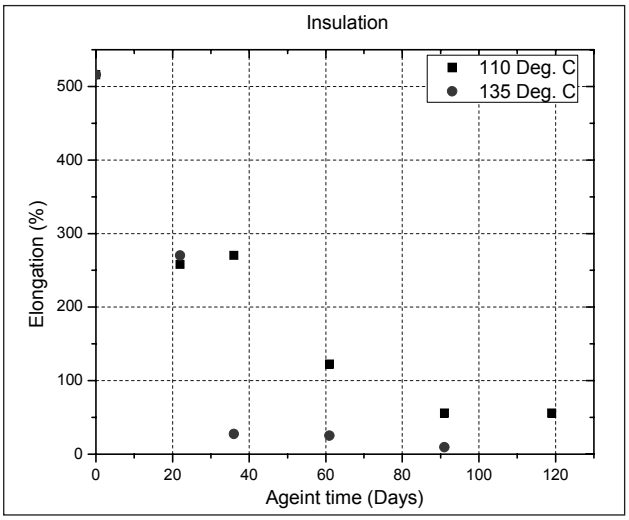

Figure-9 EAB versus ageing time of insulation

The samples were prepared from insulation and sheath materials and thermal ageing experiments were conducted in forced air circulating ovens at temperatures from 110 to 150^{0}C to simulate the field ageing. The test temperatures were selected based on the guidelines suggested in IEC 60216 [21]. The samples were taken out periodically to perform EAB and OIT/OITp measurements. The samples aged at 150^{0}C were become brittle within 12 days and were not useful for performing tensile testing and DSC measurements.

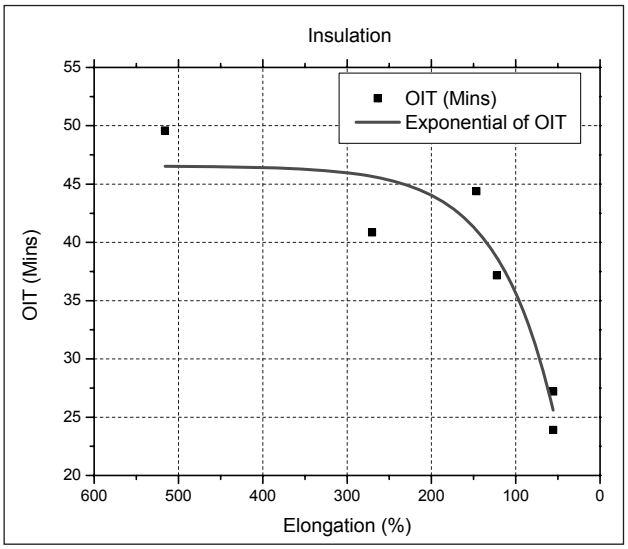

Figure-10 Exponential fit of OIT

2) *Measurement of OIT and OITp:* The OIT measurements were carried out in the range from 180^{0}C to 220^{0}C, and up to 8 hours on fresh and thermally aged polymeric samples. Additionally, OITp measurements were carried out on these samples. The procedure employed in calculating the OIT from OITp for radiation ageing was adopted for thermal ageing data as well. The calculated OITs corresponding to experimental OITp of thermally aged signal cable insulation at 110^{0}C and 135^{0}C are shown in Figure-8.

3) *Determination of elongation at break:* The EAB measurements on thermally aged cable insulation materials were performed. The mean EAB values for 110^{0}C and 135^{0}C are shown in Figure-9.

4) *Correlation:* Since tensile testing is being a benchmark technique for condition assessment of polymeric materials, the DSC findings need to be correlated with the EAB. The experimental data was analyzed to derive an empirical model for OIT. An exponential fit of OIT as a function of EAB with coefficient of determination being 0.93 for 110^{0}C condition is shown in Figure-10.

By comparing the Figure-5 and Figure-10, it is evident that the radiation ageing affects the chemical structure of the polymer resulting decrease in the thermo-oxidative stability while degrading the mechanical properties at much slower rate. However, under thermal ageing the mechanical properties degrade at higher rate as compared to the chemical properties. Hence, in remaining life assessment studies, appropriate property may be chosen under specific ageing mechanism.

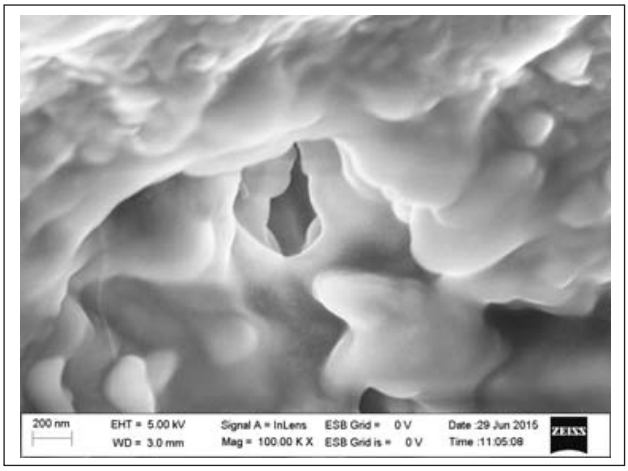

Figure-11 SEM image of un-aged insulation

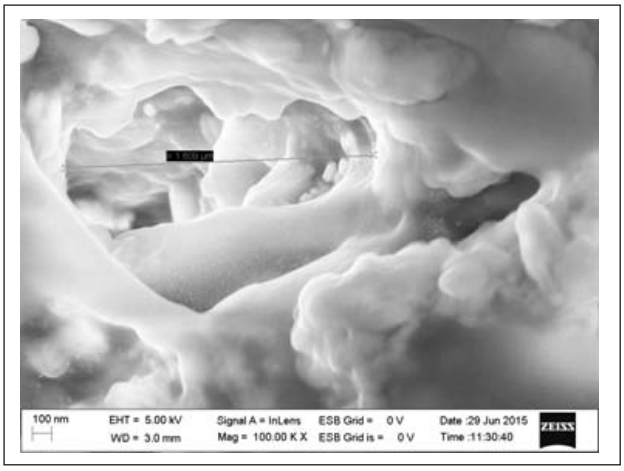

Figure-12 SEM image of insulation at 10MR

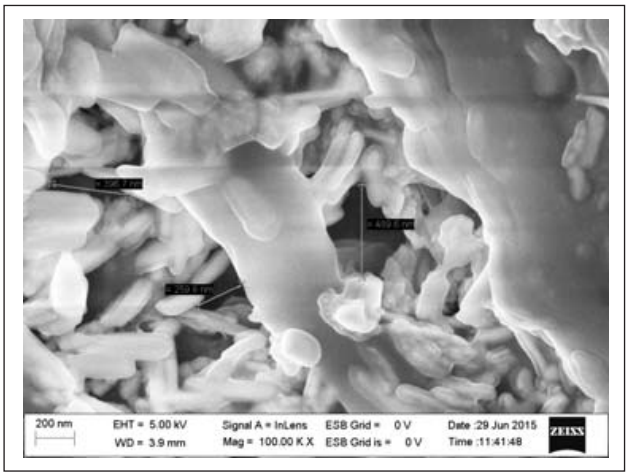

Figure-13 SEM image of insulation at 25MR

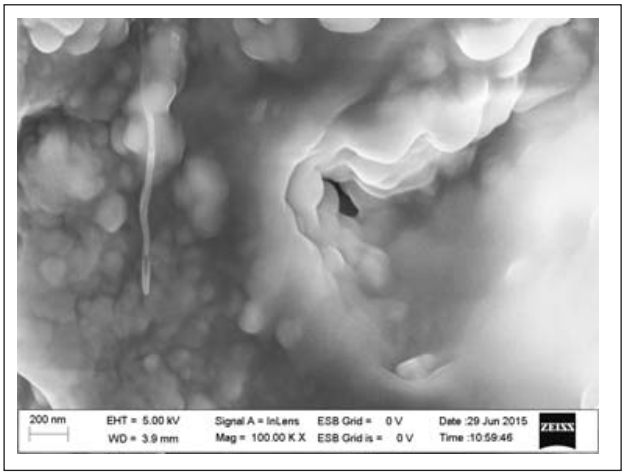

Figure-14 SEM image of un-aged sheath

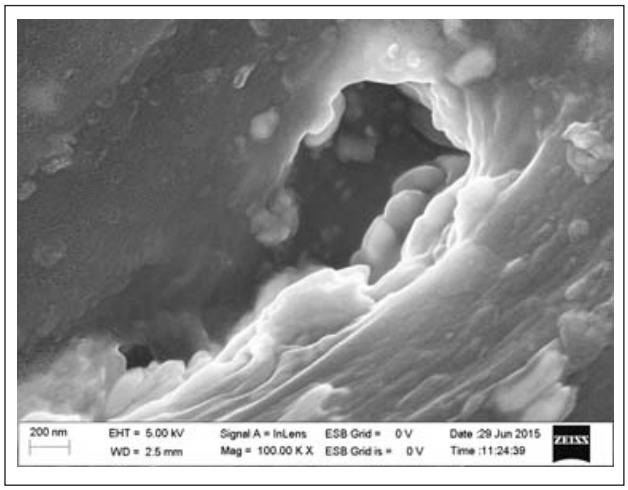

Figure-15 SEM image of sheath at 10MR

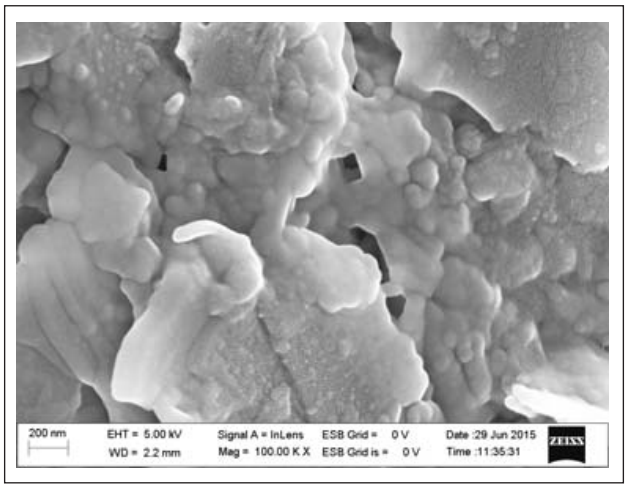

Figure-16 SEM image of sheath at 25MR

4. Scanning Electron Microscopy

Scanning electron microscopy (SEM) has become a powerful technique in materials research. Electron Microscopes are scientific instruments that use a beam of highly energetic electrons to examine objects on a very fine scale. This examination can yield information about the topography, morphology, composition and crystallographic information [22]. Field emission scanning electron microscopy (FESEM) is used to visualize very

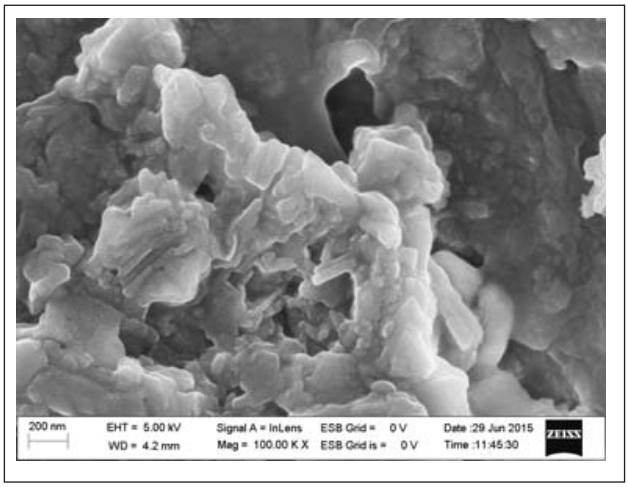

Figure-17 SEM image of sheath at 50MR

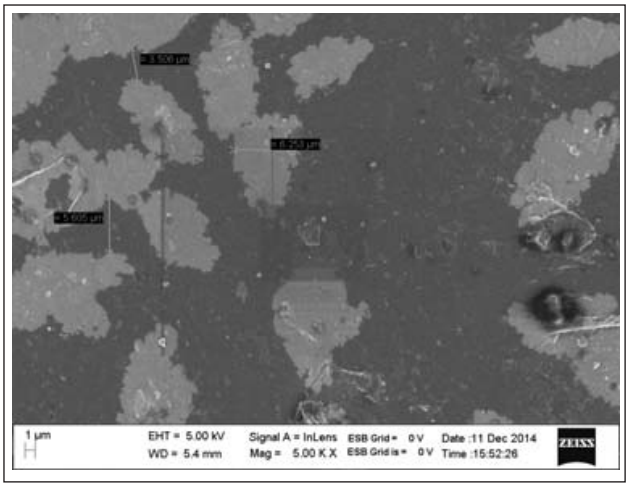

Figure-18 SEM image of un-aged insulation

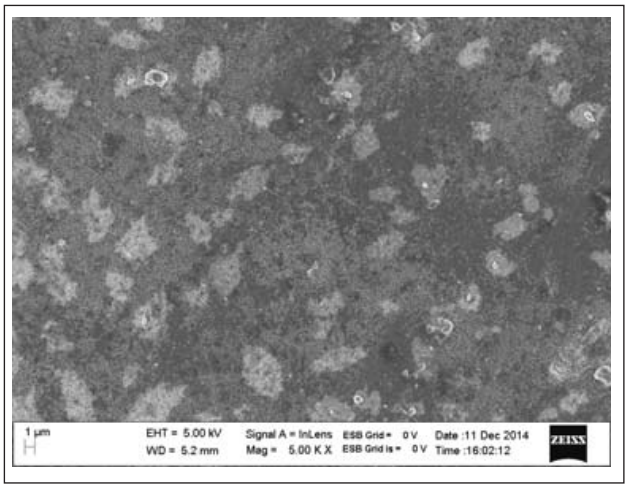

Figure-19 SEM image of insulation at 110^{0}C after 36 days

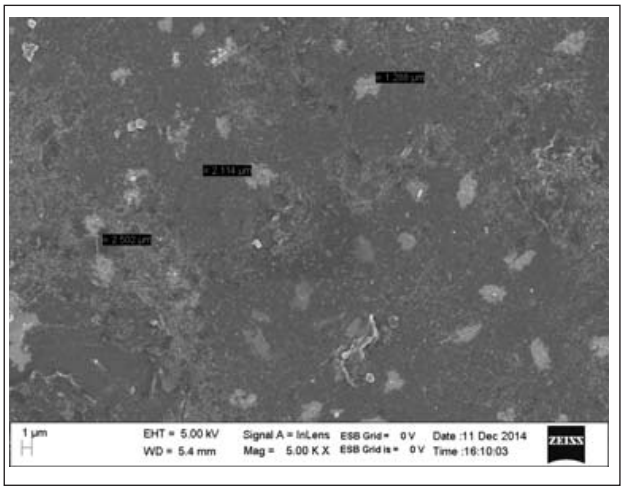

Figure-20 SEM image of insulation at 135^{0}C after 22 days

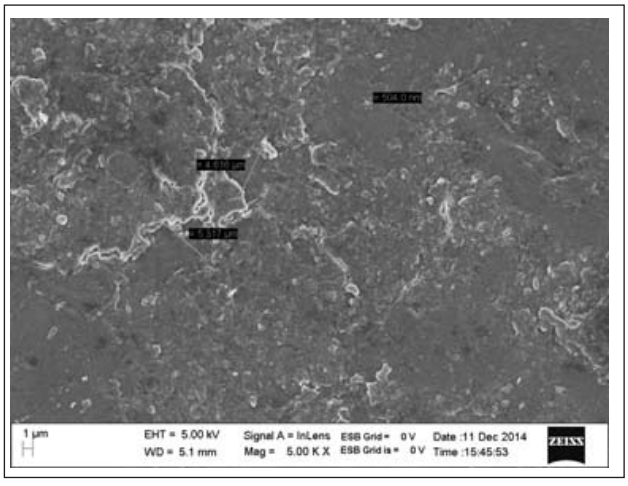

Figure-21 SEM image of un-aged sheath

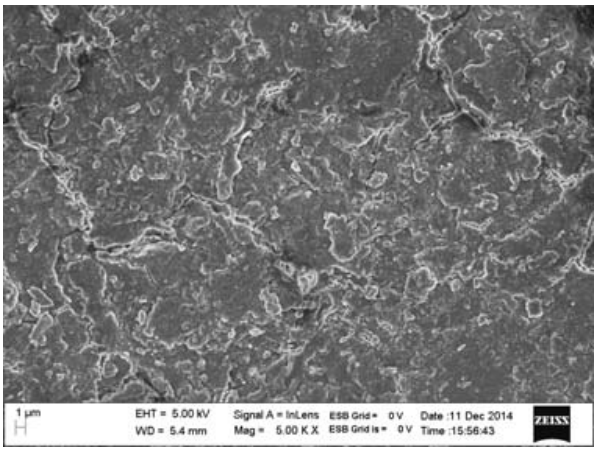

Figure-22 SEM image of sheath at 110^{0}C after 36 days

small topographic details on the surface or entire or fractioned objects.

In order to monitor the state of the un-aged and radiation aged cable insulation, the samples of the solid insulating materials mentioned in Table 1 were observed under SEM. In order to be observed with a SEM the samples were first made conductive for current by coating them with an extremely thin layer

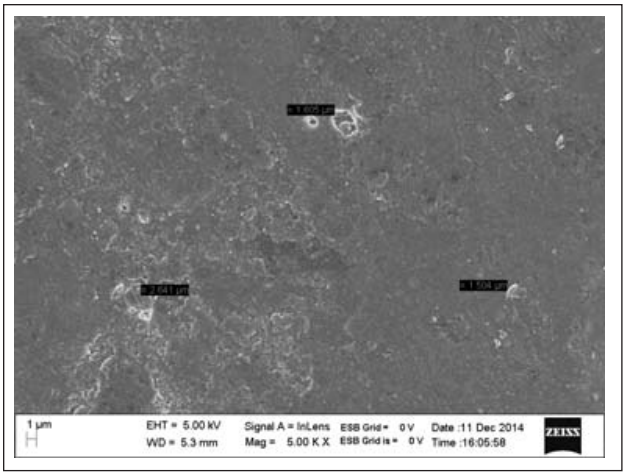

Figure-23 SEM image of sheath at 135^{0}C after 22 days

(1.5 - 3.0 nm) of gold. The SEM images for fresh and aged cable insulation and sheath are shown in Figure 11-16.

The SEM images of thermally aged and fresh samples of the cable insulating materials mentioned in Table 2 are shown in Figure 18-23.

The SEM images show a significant reduction in the elastic property (more brittle towards higher doses) in both insulation and sheath material under radiation ageing. This is to the presence of micro voids generated during the gamma radiation. The SEM images of thermally aged samples also indicate the similar effect; however, this is subjected to thermo-oxidative effect caused by thermal ageing.It can be concluded that the SEM findings support the correlations between EAB and OIT measurements. Hence, the OIT predictions may be useful in predicting the life of I&C cables.

5. Conclusions

Accelerated thermal and radiation ageing of I&C cable insulation materials has been carried out and the degradation was assessed using chemical and mechanical measurements. From the data analysis, it was found that an exponential degradation phenomenon takes place under both thermal and radiation ageing. However, the rates of degradation are significantly different in both the cases. It is also evident from the experimental evaluations that, the radiation ageing affects the chemical structure of the polymer resulting decrease in the thermo-oxidative stability while degrading the mechanical properties at much slower rate. However, under thermal ageing the mechanical properties degrade at higher rate as compared to the chemical properties. Also, the SEM findings support the correlation between EAB and OIT. Hence, in remaining life assessment studies, appropriate property may be chosen under specific ageing mechanism.

References

1. Robert J. Lofaro, Edward Grove and Peter Soo, "An evaluation of condition monitoring techniques for low-voltage electric cables", BNL-NUREG-67389, Upton, New York.
2. IAEA-TECDOC-932, "Pilot study on the management of ageing of instrumentation and control cables", International Atomic Energy Agency, 1997.
3. K. Anandakumaran, W. Seidl and P.V. Castaldo, "Condition assessment of cable insulation systems in operating nuclear power plants", IEEE Transactions on Dielectrics and Electrical Insulation, vol. 6, no. 3, pp. 376-384, 1999.
4. M. J. Jacobus, "Aging, condition monitoring, and loss-of coolant accident tests of class 1E electrical cables: Ethylene propylene rubber cables", NUREG/CR-5772, SAND91-1766/2, Vol. 2, 1992.
5. M. Ekelund, H. Edin and U.W. Gedde, "Long-term performance of poly (vinyl chloride) cables. Part 1: Mechanical and electrical performances", Polymer Degradation and Stability, vol. 92, pp. 617-629, 2007.
6. S.G. Burnay, "An overview of polymer ageing studies in the nuclear power industry", Nuclear Instruments and Methods in Physics Research B, Vol. 185, pp. 4-7, 2001.
7. R. Clavreul, "Ageing of polymers in electrical equipment used in nuclear power plants", Nuclear Instruments and Methods in Physics Research B, vol. 151, pp. 449-452, 1999.
8. L. R. Mason and A. B. Reynolds, "Comparison of oxidation induction time measurements with values derived from oxidation induction temperature measurements for EPDM and XLPE polymers", Polymer Engineering and Science, vol. 38, no.7, pp. 1149-1153, 1998.
9. S.B. Dalal, R.S. Gorur and M.L. Dyer, "Aging of distribution cables in service and its simulation in the laboratory", IEEE Transactions on Dielectrics and Electrical Insulation vol. 12, no. 1, pp. 139-146, February 2005.
10. C. Kröhnke, Polymer Science: A Comprehensive Reference. Elsevier, 2012, vol. 8.14-Polymer Additives.
11. K. T. Gillen and R. L. Clough, Predictive aging results for cable materials in nuclear power plants", Sandia Laboratories, Tech. Rep., 1990.
12. International Atomic Energy Agency, "Stability and stabilization of polymers under irradiation", 1997.
13. G. C. Stone, "The statistics of ageing models and practical reality", IEEE Transactions on Electrical Insulation, Vol. 28, No. 5, pp. 716-728, 1993.
14. NUREG/CR-6704, "Assessment of environmental qualification practices and condition monitoring techniques for low voltage electrical cables", Brookhaven national laboratory, February 2001.
15. M. Schmid, A. Ritterand S. Affolter, "Determination of oxidation induction time and temperature by DSC: Results of round robin tests", Journal of Thermal Analysis and Calorimetry, vol. 83, no. 2, pp. 367–371, 2006.
16. Y.T. Hsu, K.S. Chang-Liao, T.K. Wang and C.T. Kuo, "Correlation between mechanical and electrical properties for assessing the degradation of ethylene propylene rubber

cables used in nuclear power plants", Polymer Degradation and Stability, vol. 92, pp. 1297-1303, 2007.

17. G.V Gordon, C. Shen and M.T. Shaw, "A method for correlating natural ageing data and its application to insulation ageing in nuclear power plants", pp. 694-699,
18. INTERNATIONAL ELECTROTECHNICAL COMMISSION, "Guide for determining the effects of radiation on insulating materials. Part 1: Radiation interaction and dosimetry", IEC 544-1 (1995); "Part 2: Procedures for irradiation and test", IEC 544-2 (1991); "Part 4: Classification system for service hi radiation environments", IEC 544-4, Geneva (1985).
19. ASTM D 3895, "Test Method for Oxidative Induction Time of Polyolefins by Thermal Analysis," ASTM International.
20. ASTM D638, "Standard Test Method for Tensile Properties of Plastics," ASTM International.
21. IEC 60216, "Guide for the determination of thermal endurance properties of electrical insulating materials", 4th issue (1990-1994).
22. L. Reimer and P.W. Hawkes. Scanning Electron Microscopy: Physics of Image Formation and Microanalysis, Berlin (DE), Springer-Verlag, 2010.

Life Cycle Reliability and Safety Engineering
Vol.4 Issue 3 (2015) 25-35

Reliability Estimation by Accelerated Life Testing

V.N. Achutha Naikan
Reliability Engineering Centre, Indian Institute of Technology, Kharagpur, INDIA
Email: naikan@hijli.iitkgp.ernet.in

Abstract

The concepts of accelerated life tests, various methods of accelerations, the mathematical models for quantification of test data, procedure for evaluation of acceleration factors, failure time distributions and parameter estimation are presented in this paper. The basic concepts of Highly Accelerated Life Tests (HALT) and Highly Accelerated Stress Screening (HASS) are also covered to familiarize the latest developments in these areas. The challenges, advantages and limitations of these techniques are discussed.

A case study of high temperature accelerated life tests conducted on electrolytic capacitors is presented to illustrate these techniques. The failure criterion is the failure mode 'change of capacitance value'. The accelerated life tests were conducted at 85^{0}C, 100^{0}C and at 110^{0}C. The capacitors were charged with the rated voltage of 24 V DC during the high temperature tests. The aim of these tests was to evaluate the failure rate, mean time to failure (MTTF), acceleration factors, reliability and their variation with temperature. The test results were also used for validating the Arrhenius model for high temperature tests on electrolytic capacitors and evaluation of the activation energy. The paper is presented in such a way as to motivate the practicing reliability engineers to plan, design, and conduct accelerated life tests, and become familiar with the data analysis procedures for reliability estimation.

Key Words: Accelerated life test, Arrhenius model, Activation energy, Acceleration factor

1. Introduction

During the conceptual and detailed design stages, the failure rate and mission reliability of a component or product is predicted based on data published in reliability data handbooks. A specific design is accepted or rejected based on this prediction. The error in such predictions prediction is considerable because several assumptions are made in these models. Therefore, for high reliability applications, it is very appropriate and important to conduct life tests for reliability estimation as accurate as possible. However, life testing should be practically feasible and economically viable as an alternate method for data generation and reliability estimation in reasonable time with acceptable accuracy. Accelerated life testing (ALT) appears to be a feasible technique in such situations.

ALT is conducted to generate sufficient failure data in short time. This is practically done by increasing stress levels on components. It is found that the failure rate increases very fast, in many cases exponentially, with applied stresses. This philosophy is effectively used for testing engineering components and systems which will require long periods of testing at normal stress conditions. Since, at the product development stage one cannot wait for such a long duration, the only option available is ALT for quick feedback. This is illustrated in the figure-1.

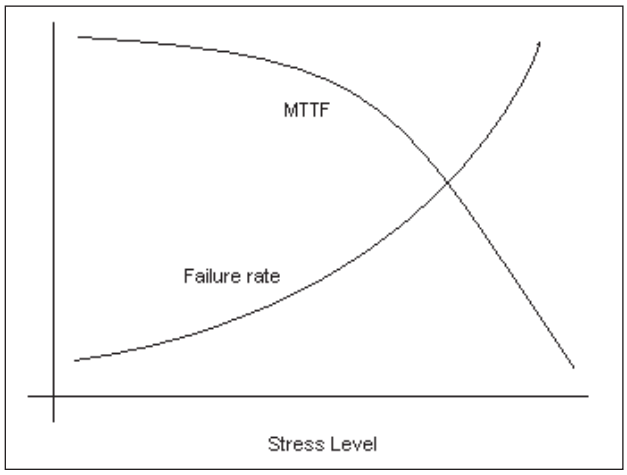

Figure 1: Failure rate, MTTF and stress level

Temperature, voltage, current density, humidity, dust, salt spray, corrosive atmosphere, mechanical stresses, electrical stresses, hydraulic pressure, shock,

vibration, friction (lack of lubrication), cyclic stress, chemical accelerators (catalysts), oxidizers or any other circuit or system parameter can be used for acceleration of failure rate of component or system under test. In many cases a combination of stresses can provide very good results. Based on the data collection, ALT can be classified as Accelerated Binary Tests, meaning failed/not failed [1]; right censored (test terminated before all item failure) or interval censored (failures are recorded at particular intervals) [2]; Accelerated Repeated Measures Degradation Tests (degradation on a sample of units at different points in time [3] and Accelerated Destructive Degradation Tests (only one observation per test unit) [4].

Another method to accelerate failures is by increasing the duty cycles. For example, an industrial push button switch generally is operated (on/off) a few cycles a day. The failures of this can be accelerated by operating these switches several cycles per day in a switch testing machine. This is generally known as compressed time test in literature.

2. ALT Implementation

The success of accepting ALT as a strategy for reliability estimation of products depends on several factors. Several technical, economic, statistical, managerial factors must be considered to implementing a successful ALT program. Some important factors generally considered are discussed below.

Sample Size: In general, sample size of 30 items is statistically significant, correctly representing the population. In actual practice we also need to consider other factors such as the availability of resources, cost of items and conduction of tests, and accuracy required. A trade off study may be conducted prior to deciding the sample size.

Test Chambers/facility: Accelerated life tests are conducted in environmental chambers such as dry heat chamber, temperature cycling or temperature humidity chamber. These chambers should have the capability to hold the required accelerated stress levels for the required duration. There should be adequate space for keeping the test items inside the chambers without physical contact with the chamber walls, so that the stresses are uniformly applied from all directions. Temperature stress should not be applied by conduction; but by convection. There should also be facility for simultaneous application of electrical voltage to the test items using a power source generally kept outside the test chamber. For accelerating mechanical components, we may need to use special facilities capable of accelerating the failures by applying static or dynamic loads and higher speeds.

Test Fixtures: Test fixtures are required for properly keeping the test items inside the chamber such that the test items are all subjected to approximately same level of stress. Test items need to be firmly fixed so that there is no physical movement during the test and there is sufficient space between the items. Each type of component may require a different text fixture. Designing, and manufacturing text fixtures are important activities prior to conducting the accelerated life test.

Stress Levels: Decide the appropriate stress levels for acceleration. Conduct life tests on these items at least for three different high stress levels. The stress levels should not be too low or too high. A pilot step stress testing can be performed on a few samples to identify the applicable levels of stresses for correct acceleration. Too low stress level may not truly accelerate failures whereas too high stresses may result in change of failure mechanism.

Failure Mechanisms: After conducting these tests, carefully check the failure mechanisms at all stress levels and also that at use conditions. If the failure mechanisms match significantly then try to derive a quantitative relationship of life with applied stress. If the failure mechanisms do not match, then these failure data have no significance and therefore cannot be used for any quantification or prediction. In such cases either the test can be repeated or the type of stresses can be changed for subsequent tests.

Test Duration: Ideally, test duration should be such that at least 50% of the items under test fail. These are failure censored tests. The tests may be also be time terminated. For this, initial activation energy can be assumed for the component failures based on either standards or experience. The required test duration at a test temperature stress can be estimated based on this.

Data Analysis: The data generated in accelerated tests consist of failure times (or number of failures in a test duration, if failure times are not collected individually) at each stress level. Analysis of these data requires two steps. In the first step, the failure data at each stress level is fitted to a best fit statistical distribution and the parameters are estimated. The MTTF, failure rate, and other reliability parameters at each stress level can be computed from these

estimates. In the second step, an acceleration model is used for relating the computed MTTF or failure rate between the stress levels. Arrhenius model, Eyring model, Inverse Power Law Model, Temperature-Humidity Model, Temperature Non-Thermal Model, and Multivariable Relationships: General Log-Linear and Proportional Hazards, and Time-Varying Stress Models can be used for this purpose.

Operational Reliability: Acceleration models can be used for evaluating acceleration factors between stress levels. Using this procedure, the reliability parameters such as MTTF and failure rate at operational stress level can be extrapolated.

This procedure may appear very simple, but in actual practice it is not. The most difficult and important part of the procedure is the method of identifying failure modes and the subsequent quantification of data for extrapolation. It is clearly wrong to use data on one failure mode to estimate failure rate of the component in another mode. Another important task is the selection of the most appropriate models for ALT data analysis.

3. ALT Data Analysis

As mentioned earlier, ALT data analysis comprises two important stages. ALT data consists of failure times of components at different stress levels. Therefore, the first task is to find out the most appropriate distribution for the failure times at each of the stress levels. If we get the same type of distribution at all these stress levels, it indicates that the failure mechanisms are likely to be same. If the shape parameter at different stresses is approximately same, it confirms the failure mechanisms to be same. In the next stage, a correct acceleration model needs to be selected to relate the reliability parameters at different stress levels. These are discussed in more details in the following sections.

3.1 Life Distribution and Parameter Estimation

The ALT data at each stress level will follow one of the continuous probability distributions such as exponential, Weibull, normal, lognormal, etc. The first step in data analysis is to find out the best fit distribution of the data at a given stress level and to estimate the distribution parameters. Analytical methods such as MLE, LSE, or Moment Estimators with adequate type of goodness of fit statistics such as χ^2 test, Mann's test, Bartlett's test [5] can be used for this. Simple graphical method using the probability papers can also be used for this. Alternately, software packages such as MINITAB, Easy fit, and Weibull $^{++}$ can be used. Failure rate of the tested components can be estimated based on the selected distribution using the fundamental reliability equations. For example, failure rate at any stress level is equal to the ratio of probability density function to the reliability function at that stress level.

$$h(t) = \frac{f(t)}{R(t)}$$

This procedure can be repeated for all stress levels to estimate the mean life (MTTF) and hazard rates at all stress levels. The acceleration factor between any two levels of stress can be estimated from the estimated mean life at various stress levels as discussed in the subsequent sections of this paper.

3.2 Life-Stress Relationship

The next step is to establish a mathematical relationship between failure rate and stress level. This can be done by selecting an appropriate acceleration model presented below. Alternatively, a single or multivariate regression model can be developed from the expected life and stress matrix obtained in the previous step. Important acceleration models available in the literature are briefly discussed in this section. [6, 7, 8, 9, and 10] are good references for further details.

3.2.1 Arrhenius Model

The Arrhenius model is used when the stress applied for acceleration is only temperature. According to Arrhenius law, rate of simple chemical reaction depends on temperature as follows [1, 11, and 9].

$$rate = A' \exp\left(-\frac{E_a}{kT}\right)$$

where T : temperature T^0K

E_a: activation energy of the failure mechanism of the component (eV)

k : Boltzman's constant = $8.6171 * 10^{-5}$ eV/ ^0K

A′ : constant

The product fails when the critical amount of amount of chemical has reacted. This suggests that the expected time to failure (τ) of the item is inversely proportional to the rate. Thus we get the Arrhenius relationship

$$\tau = A \exp\left(\frac{E_a}{kT}\right)$$

Where, A is a constant that depends on product geometry, specimen size and fabrication, test method and other factors. Products with more than one failure mode, have different A and E_a values for each mode [2].

3.2.2 Eyring Model

The Eyring relationship was formulated from quantum mechanics principles. Most often used when the thermal stress (temperature) is the acceleration variable. It is often used as an alternative to the Arrhenius model [9, 2]. The Eyring model can be written as follows

Expected life, $\tau = (A/T)\exp[B/kT]$

Where, A and B are constants characteristics of the product and test method, k: Boltsman's constant and T is Temperature (^oK). For small range of absolute temperature, (A/T) is constant, and the above equation is close to Arrhenius relationship [2].

This equation is sometimes modified for combined temperature (T) and another stress (V) application. Thus a Generalized Eyring model can be written as follows [2]

Expected life,

$$\tau = (A/T)\exp[B/kT]\times\exp\{V[C+(D/kT)]\}$$

Where, A, B, C and D are constants to be estimated from data. It can be seen that there is an additional part compared to the simple Eyring relationship to account for the effect of the second stress.

3.2.3 Inverse Power Law Model

Increasing the voltage at which the test units are operated often accelerates failures of electrical equipments. Following power law is used in modeling such stress accelerations

$$= \left(\frac{V_A}{V_N}\right)^n$$

Where V_A and V_N are accelerated and normal use voltages. t_A and t_N are accelerated and normal test durations. n is another model parameter to be determined. (n = 2 to 5 is a reasonable value of power)

3.2.4 Temperature-Humidity Model

Combined temperature and humidity is an excellent method for acceleration of failures of electronic components. A model for combined temperature and humidity stress is given below [2]

$$\tau = A(RH)^{-n}exp[E/kT]$$

Where, RH is the relative humidity. Several forms of this model are in the literature. A number of different humidity models are reviewed and compared by [3, 9]. For more details on ALT applications involving temperature and humidity [12, 9, and 13] can be referred.

3.2.5 Temperature Non-Thermal Model

When temperature and a second non-thermal stress (*e.g.* voltage) are the accelerated stresses of a test, then the Arrhenius and the inverse power law relationships can be combined to yield the temperature-non thermal (T-NT) relationship as presented below.

$$L(U,V) = \frac{C}{U^n e^{-\frac{B}{V}}}$$

Where, U is the non-thermal stress (*i.e.* voltage, vibration, etc.), V is the temperature (in absolute units), B, C, and n are the parameters to be determined using test data.

3.2.6 Temperature Cycling

It is possible to accelerate thermal cycling failure modes by increasing either the frequency or amplitude of the cycles (increasing amplitude generally increases mechanical stress). The most commonly used model for acceleration of thermal cycling is the Coffin-Manson relationship as given below.

$$N = \frac{\delta}{(\Delta_{\text{temp}})^{\beta_1}}$$

where Δ_{temp} is the temperature range δ and β_1 are properties of the material and test setup as suggested by [4]. This power-rule relationship explains the effect that temperature range has on thermal-fatigue life cycles-to-failure distribution. This relationship is used for both mechanical as well as electronic components. Suggested β_1 value varies from 2 (for metals) to 5 (for microelectronics) [2].

3.2.7 Multivariable Relationships: General Log-Linear and Proportional Hazards

The life-stress relationships presented so far have been either single stress relationships or two stress relationships. In most practical applications however, life is a function of more than one or two variables (stress types). In addition, there are many applications where the life of a product as a function

of stress and of some engineering variable other than stress is sought. General Log-Linear Relationship and Proportional Hazard models are examples. When a test involves multiple accelerating stresses or requires the inclusion of an engineering variable, a general multivariable relationship is needed. Such a relationship is the general log-linear relationship, which describes a life characteristic as a function of a vector of *n* stresses, or $X = (X_1, X_2 \ldots X_n)$. For details readers may refer [2].

3.2.8 Simple use-rate acceleration models

In these models, if the cycles-to-failure distribution does not depend on the cycling rate, one can use the following relationship.

$$AF\ (use\ rate) = \frac{Use\ rate}{Accelerted\ use\ rate}$$

The failure of rolling bearings can be accelerated by running them at 3 or more times the normal speed (Nelson, 1990) and the cycles-to-failure of electrical insulation can be shortened by a factor of AF(412) = 412/60 when the applied AC voltage in endurance tests was increased from 60 Hz to 412 Hz (Johnston et al.1979). In fatigue testing the crack growth rate increased as per the following empirical power-rule relationship (Dowling, 1993)

$$AF\ (use\ rate) = \left(\frac{Use\ rate}{Accelerted\ use\ rate}\right)^p$$

where p is a constant. Miner's rule is used to predict life in which system components are exposed to varying stresses (Nelson, 1990). Increased cycling rate may however increase temperature and will affect the cycles-to-failure distribution. This is especially true if there are effects like creep-fatigue interaction (Dowling, 1993). Similarly, changes in cycling rate would affect the distribution of lubricant on a rolling bearing surface.

3.3 Acceleration Factor

Acceleration factor (AF) is another term associated with accelerated life tests. This is defined as the ratio of expected life at normal operating temperature to the expected life at accelerated temperature. Following relationship can be used.

$$AF = \frac{MTTF(T_N)}{MTTF(T_A)}$$

Where $MTTF(T_A)$ and $MTTF(T_N)$ are mean time to failure at accelerated and normal temperatures. From this relationship, it can be seen that for exponential failure time models (assuming that the time to failures follow exponential distribution for accelerated and normal stress conditions) acceleration factor is

$$AF = \frac{\lambda(T_A)}{\lambda(T_N)}$$

where $\lambda(T_A)$ and $\lambda(T_N)$ are failure rates at accelerated and normal temperatures. The activation energy (E_a) can be evaluated for a given failure mechanism of a component by conducting high temperature life tests at two different temperatures and then applying Arrhenius model. The acceleration factors for different models are presented in the table.

Table 1: Acceleration Factors for different models

Model	Acceleration factor
Arrhenius Model	$AF = Exp\left[\frac{E_a}{K}\left(\frac{1}{T_n} - \frac{1}{T_A}\right)\right]$
Eyring Model	$AF = \left(\frac{T_A}{T_N}\right)\exp\left[\frac{E_a}{K}\left(\frac{1}{T_N} - \frac{1}{T_A}\right)\right]$
Inverse Power Law Model	$AF = \left(\frac{V_A}{V_N}\right)^n$
Use-rate models	$AF\ (use\ rate) = \left(\frac{Use\ rate}{Accelerted\ use\ rate}\right)^p$
Temperature-Humidity Model	$AF = Exp\left[\frac{E_a}{K}\left(\frac{1}{T_N} - \frac{1}{T_A}\right) + B\left(\frac{1}{H_N} - \frac{1}{H_A}\right)\right]$
Temperature Non-Thermal Model	$AF = \left(\frac{U_A}{U_N}\right)^n e^{B\left(\frac{1}{V_N} - \frac{1}{V_A}\right)}$

4. The Concepts of HALT and HASS

Main objective of traditional life testing is reliability, MTBF and failure rate estimation of engineering components and systems. However, the objective of HALT is to forcefully precipitate the presence of any latent faults in the component or system. No quantification is done and product ruggedization is the focus of HALT. It is generally conducted on the design prototypes during product development phase to find out weak links in the design and fabrication process. All-axis simultaneous vibration, high-rate, broad-range temperature cycling, power cycling, voltage and frequency variation, humidity, and any other stress that may expose design or process problems can be used. Nelson (1990) describes such tests as "elephant tests" and outlines some important issues related to these.

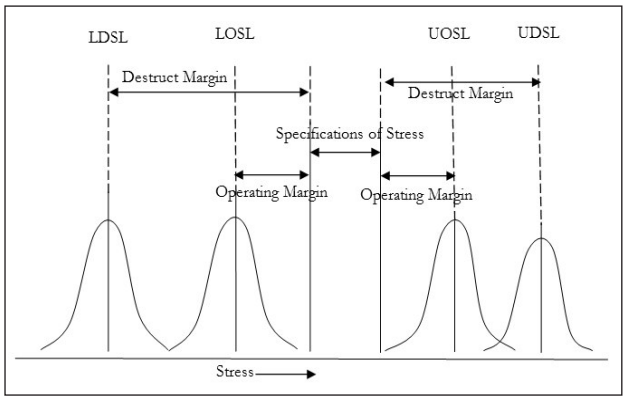

Figure 2: Stresses for HALT

HALT is generally conducted on a product in an iterative step-stress method. Here the test starts with subjecting the products under the operational stress limits for some time till some failures occur. These failures are now analyzed and new products are made by improved design and manufacturing process. The HALT stress is now increased to the next step and the procedure is repeated till the stress level reaches the destructive stress limits, (or the technology limits). A few samples of the final product are again subjected to the highest stress levels for further verification and validation. In this way, the products are made rugged and highly reliable. HALT decides the technological limitations of the product whereas ALT determines the MTBF of the product.

Highly accelerated stress screening (HASS) is a method for screening of products using stresses which are substantially higher than the normal operational, storage, and transportation stresses. A well designed HASS will ensure 100% screening and leave the products with majority of life remaining with them after screening. In most situations two stage screening tests are carried out; viz., first the precipitation HASS and then an immediate detection HASS. This is to make sure that all precipitated faults are detected, analyzed, and then corrected. Precipitation HASS can be run beyond operation stress limits of the product. Detection HASS with simultaneous application of different stresses (with vibration as an essential stress) is found to be very effective. HASS should be done only on the products, which have already been made rugged by a series of HALT cycles. Otherwise, HASS may induce latent faults on products that may surface in the field. If HALT is followed by HASS, the field reliability can be substantially improved. HASS is conducted only after a product undergoes HALT procedure and made rugged. Otherwise, HASS will be counterproductive. This is because HASS is conducted at higher stress levels which a normal product may not be passed through without substantial induced damages. The stress levels for precipitation HASS is generally above the operational stress levels of the product so as to achieve time compression and cost reduction. Detection HASS is generally performed at lower stress levels compared to precipitation HASS. Six-axis vibration shaker at low GRMS in combination with another stress like temperature is found to be very effective for detection screening. For more details about HALT and HASS refer [9, 11].

5. Case Study

As discussed earlier, temperature has a major influence on the reliability of electronic components because of the accelerating effect of increasing temperature on almost all failure mechanisms. This phenomenon is used judiciously for conducting accelerated life tests with the objective of generating data in small test duration. The data thus generated is analyzed using mathematical models like Arrhenius model [2] and then the results are extrapolated to the normal operating temperature for evaluation of various reliability parameters. However, the model used should be experimentally verified for each type of component and failure mechanism for ensuring its validity. Otherwise the results can be quite misleading [1]. Data from MIL-HDBK-217F [11] is generally used to examine the temperature dependence of failure rates of electronic components in actual usage, (but its dependence is much smaller than expected from the published values of activation energies of component failure mechanisms), or assumed in some commonly used thumb rules. One reason for

this smaller dependence is that the studies generally have been carried out at temperatures much higher than the component field operating temperature, so that high activation energy mechanisms have become more predominant at these temperatures.

It is common practice in electronic industry to assume the Arrhenius model [2], with fixed parameters, to be closely connected with well defined failure mechanisms, for example electro-migration and corrosion. Therefore for different failure mechanisms the values of the activation energies are determined and suggested for general use in accelerated life tests [6]. On the other hand, warning of indiscriminate application of fixed values is made because:

1. The scientific background of Arrhenius model does not allow application over a wide range of temperature [12].
2. Experiments have shown that activation energy depends additionally on various other factors [1, 2].
3. Even small variations in activation energy can cause considerable inaccuracy in reliability prediction using data from accelerated life tests [12].
4. The applicability and validity of Arrhenius model should be studied for a given component and failure mechanism before using it for reliability evaluation

Hence there is a need to gather information and to estimate the parameters of Arrhenius model with sufficient accuracy. In this case study, the aim is to conduct accelerated life test on aluminum electrolytic capacitors for estimation of the reliability parameters. The stress applied is high temperature. One of the aims of this study is also to check the validity of the Arrhenius model for these capacitors. As discussed earlier, an important factor to be considered here is that the failure mechanism should not change for both these temperatures.

The accelerated life test data at each temperature can be fitted to a best fit distribution and the distribution parameters can be estimated using the standard procedure. The failure rate at each temperature can thus be established. Let $MTTF_1$ and $MTTF_2$ represents failure rates at temperatures T_1 and T_2. If ($T_1 < T_2$), then acceleration factor between these two temperatures is:

$$AF = \frac{MTTF_1}{MTTF_2}$$

From this relationship E_a can be evaluated. If we conduct tests at a few different temperatures we can evaluate the value of E_a for any two combinations of temperatures. If the E_a values are same (within the limits of experimental error) it can be concluded that the failure mechanism of the component under investigation can be represented by the Arrhenius model with activation energy equal to the mean of activation energies evaluated for all combinations of the test data. This is the philosophy followed in this experimental study.

5.1 Experimental Setup

The experimental setup for high temperature test on electrolytic capacitors is simple and consists of the following:

Dry Heat Chamber: This is the chamber in which the component to be tested is subjected to high temperature. The inside of the chamber has a wire mesh over which the capacitors can be kept so that they do not come in contact with the chamber walls. Care is taken to keep the components in the middle of the volume of the chamber so that temperature is uniform from all sides. A power (DC) supply is connected to the capacitors through the chamber. The chamber also has temperature controlling mechanisms. The required test temperature can be set at a pre-decided value with the help of a temperature setting knob.

Technical Specifications of the Chamber

Overall dimensions	:	183cm x 148cm x 170cm
Working Space	:	100cm x 100cm x 100cm
Approximate weight	:	1000 Kg
Operating range	:	ambient to 300 ^{0}C
Control accuracy	:	±1 ^{0}C
Air circulation	:	Vertically mounted motor and fan
Heating	:	Six U type air heaters
Power supply	:	440 V, 3phase, 50Hz

Capacitor Holder: These are aluminium rods for connecting capacitors and then placing them inside the chamber. There are two leads connecting these holders to the chamber through which an external power supply can be given to the capacitors. Apart from these a multi meter and a 24 V DC (rated voltage of the capacitors under test) power supply are also used.

5.2 Experimental Procedure

The maximum operating temperature of these capacitors is generally 85°C for standard use and 105°C

for high-temperature use; higher temperature units are available, but uncommon. In order to determine the feasible temperature range, pilot tests were conducted at a low temperature (50^{0}C) and at a high temperature (130^{0}C). Following are the results:

At 50 ^{0}C: none of the capacitors failed

At 130 ^{0}C: all of them failed.

In both cases the failure mechanism was change of capacitance value, but at 130 ^{0}C another failure mechanism namely physical damage and failure was also present in some capacitors. Therefore it was decided to carry out the actual tests at temperatures within this range (preferably at lower levels to avoid multiple failure mechanisms) and tests were conducted at 85 ^{0}C, 100 ^{0}C and at 110 ^{0}C.

Table 2: Summary of data of life testing on electrolytic capacitors

Sl. No.	Times to Failure at (in hour)		
	85^{0}C	100^{0}C	110^{0}C
1	9.3	3.7	2.1
2	33.6	6.4	2.4
3	5.1	2.0	1.1
4	2.3	0.9	0.5
5	14.5	5.6	1.2
6	8.0	3.2	1.8
7	1.6	0.6	0.4
8	5.2	2.1	Test Terminated at 2.4 hours
9	11.4	4.6	
10	19.5	4.8	
11	9.6	3.9	
12	9.3	Test Terminated at 6.4 hours	
13	4.8		
14	1.5		
15	33.2		
16	Test Terminated at 33.6 hours		

Following are the steps followed for conducting these tests:

1. 30 good capacitors (commercial off the shelf quality) with specifications of 100 ± 5μF were randomly selected for test at each temperature; 'good' means, the capacitance value within the allowable tolerance specified.
2. These are fitted parallel on the holder such that all the positive terminals are on one side.
3. These are then inserted in the dry heat chamber at room temperature and the leads from the holder are connected to a 24 V DC (rated value for these capacitors) power supply through the chamber terminals designed for this purpose.
4. The chamber is then put on (main switch, fan, controller and window light in that order)
5. The required test temperature is set by adjusting the control knobs.
6. When the temperature inside the chamber reached the set temperature, then the power supply (24 V DC) is switched on.
7. The chamber and the DC power supply are switched off after a fixed duration of testing. This duration is calculated for each test temperature by assuming a value of 0.6 eV for the activation energy of the capacitor.
8. An on line monitoring circuit is used to monitor the status of capacitors during the test.

5.3 Observations and Results

The experimental data are presented in the table 2. It consists of the times to failures of the capacitors during the high temperature accelerated tests at 85^{0}C, 100^{0}C and 110^{0}C. These data are fitted to various distributions using Weibul $^{++}$. It is found that the two parameter Weibull distribution fits best for the data at all the test temperatures. This is presented in the figure 3. The goodness of fit values the parameters of the distribution, and the MTTF at the three test temperatures are presented in the table 3.

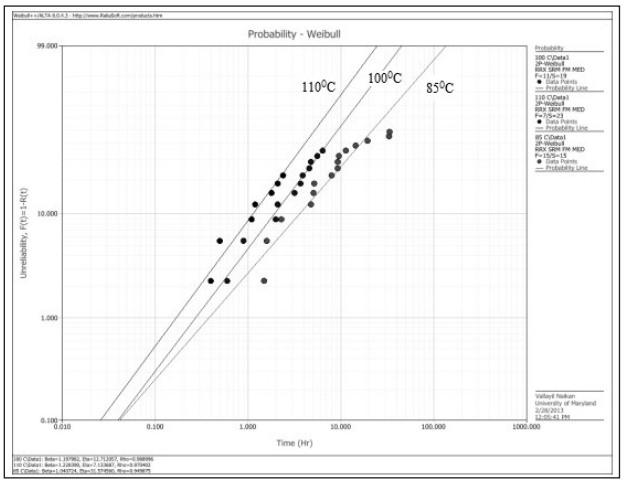

Figure 3: Weibull Distributions fitted by Weibull++

The MTTF of the capacitors at 85^{0}C, 100 ^{0}C, and 110 ^{0}C are given in the above probability plots. The corresponding failure rates can be computed by taking inverse of the MTTF. These are presented in the table 3. The AF and the activation energy at different combinations of temperatures can be computed

assuming the Arrhenius relationship discussed earlier. For example, the AF between 100 ^{0}C and 85 ^{0}C is computed as follows.

$$\mathrm{AF}(100,85) = \frac{MTTF_{85}}{MTTF_{100}} = \frac{31.57}{11.96} = 2.568$$

Activation energies for the combination of (100^{0}C and 85^{0}C) can be computed by the following equation.

$$\mathrm{AF}(100,85) = 2.568 = Exp\left[\frac{E_{a(100,85)}}{8.615 \times 10^{-5}}\left(\frac{1}{273+85} - \frac{1}{273+100}\right)\right]$$

By solving this equation we get, $E_{a\ (100,\ 85)}$ = 0.7322 eV/ ^{0}K

Similarly, the AF and the activation energies for other two combinations are computed and presented in the table 4.

Table 3: Weibull Parameters, Goodness of Fit and MTTF

Test Temperature	85 ^{0}C	100 ^{0}C	110 ^{0}C
Scale parameter (α)	31.07	12.71	7.13
Shape Parameter (β)	1.04	1.19	1.22
Goodness of Fit	0.95	0.99	0.97
MTTF	31.57	11.96	6.67

Table 4: Acceleration Factors and Activation Energies

Temperature combinations	**100 ^{0}C to 85^{0}C**	**110^{0}C to 100^{0}C**	**110^{0}C to 85^{0}C**
Acceleration factor (AF)	2.598	1.793	4.658
Activation energy (E_a) in eV/^{o}K	0.7322	0.7187	0.7270
Average Activation energy (E_a) in eV/^{o}K	0.7259		

It can be seen that all the three combinations of test temperature data give approximately the same value of E_a. The slight variation in this value may be due to:

1. Experimental error because of not considering the effect of time required for temperature building up inside the chamber from room temperature to test temperature.
2. Ideally, the shape parameters of all the three distributions should be same. There is a small variation of the values of shape parameters of the Weibull distribution in the actual case. This is because of the experimental error. An average value of shape parameter is 1.15.
3. Some of the capacitance values after the test are very near to the specification limits. This leads to some subjetiveness in deciding the failure of capacitors and thus the associated error.

From these results it can be concluded that the electrolytic capacitors under test follow Arrhenius model of temperature acceleration, within the experimental error. The average activation energy is 0.7259 eV/^{0}K. Using this value of E_a, variations in failure rate, MTTF, and reliability of these capacitors with temperature are studied.

Suppose that the operational temperature of these capacitors is at (T = 30^{0}C). Following equations can be used to compute the MTTF and the reliability function of these capacitors at 30^{0}C.

MTTF at temperature T can be computed by,

$$MTTF_{30} = MTTF_{85}\ exp\left[-\frac{0.7259}{8.615 \times 10^{-5}}\right]\left(\frac{1}{358} - \frac{1}{303}\right) = 2264\ hours$$

The relationship of the MTTF and temperature is presented in the figure 4.

Reliability at temperature the operational temperature of 30^{0}C and time t can be computed as follows. The shape parameter is expected to remain same for the Weibull distributions at all temperatures. In the present case, there is a slight variation of the shape parameter due to experimental and data collection errors. Therefore, an average value of shape parameter is computed for practical applications which is β_{30} = 1.15.

The scale parameter is computed from the following relationship.

$$MTTF_{30} = \propto_{30} \Gamma\left(1 + \frac{1}{\beta_{30}}\right)$$

Substituting $MTTF_{30}$ = 2264 hours, and β_{30} = 1.15 in the above equation we get, α_{30} = 2426.15

The following reliability function for Weibull distribution is used to compute the reliability variation at the operating temperature of 30^{0}C.

$$R_{30}(t) = e^{-\left(\frac{t}{\alpha_{30}}\right)^{\beta_{30}}}$$

The reliability function at the operational temperature is shown in the figure 5.

Once the activation energy is known, MTTF and reliability can be estimated for these electrolytic capacitors at any other operating temperature following the above procedure. Similar studies can

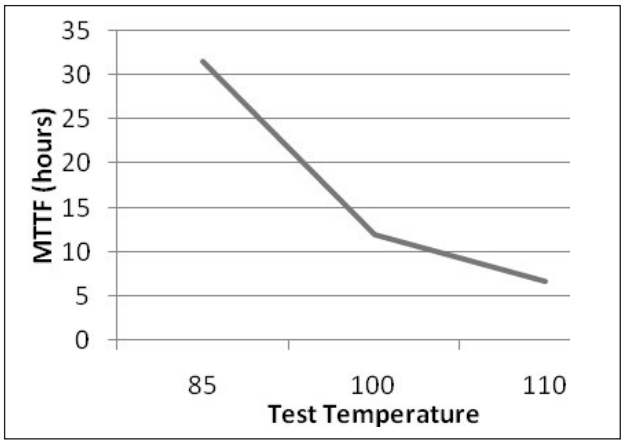

Figure 4: Failure rate Vs Temperature

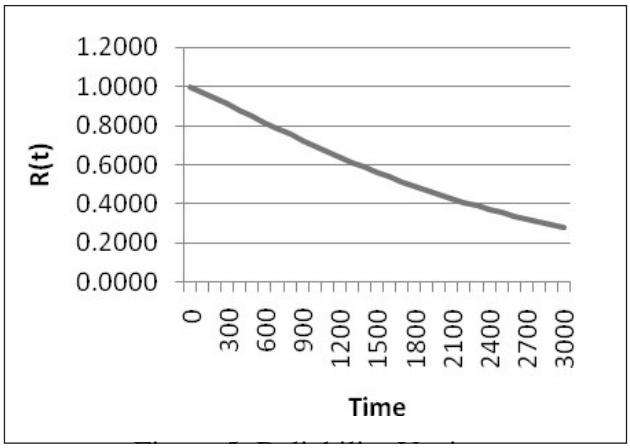

Figure 5: Reliability Vs time

be carried out on other electronic components and products. The distributions may be different in several cases, but the procedure remains the same.

6. Conclusions

This paper has presented the basic concepts of accelerated life testing, the procedure and preparation required to plan and execute the ALT, the data analysis procedures, acceleration models and some limitations. A case study on the high temperature ALT performed on electrolytic capacitors is also presented. The application of the Arrhenius model is validated for electrolytic capacitors for the failure mode "change of capacitance value". The average activation energy is 0.7259 eV/^{0}K. The MTTF and reliability of electrolytic capacitors are very sensitive to temperature, especially at higher levels. Therefore these capacitors are suitable for low temperature applications. Heat transfer and cooling mechanisms should be incorporated in the design if these are used at higher temperatures.

References

1. Blanks H. S., "The temperature dependence of component failure rate", Microelectronics and Reliability, Vol.23(2), p297-307, 1980.
2. Black J.R, "Electromigration - a brief survey and some recent results", IEEE Transactions on electron devices, Vol.16, 1989.
3. Boccaletti, G., Borri, F. R., D'Esponosa, F., and Ghio, E. (1989), "Accelerated Tests." Microelectronic Reliability, Volume II, Reliability, Integrity Assessment and Assurance, Chapter 11, edited by E. Pollino, Norwood: Artech House.
4. Dowling, N. E. (1993), Mechanical Behavior of Materials, Englewood Cliffs: Prentice Hall.
5. Escobar, Luis A. and Meeker, William Q., Planning Accelerated Life Tests with Two or More Experimental Factors, Technometrics, Vol. 37, No. 4, pp. 411-427, 1995.
6. Escobar, L. A., Meeker, W. Q., Kugler, D. L., Kramer, L. L. (2003), "Accelerated Destructive Degradation Tests: Data, Models, and Analysis," Mathematical and Statistical Methods in Reliability, B. H. Lindqvist and K. A. Doksum, Editors, World Scientific Publishing Company.
7. Hartler Gisela (1986), "Parameter estimation of the Arrhenius model", IEEE Transactions on Reliability, R-35, p414-418.
8. Hirose H (1993), "Estimation of threshold stress in accelerated life testing", IEEE Transactions on Reliability, R-42, 650-657.
9. Hobbs Ph. D., Gregg K. (2005), HALT and HASS, Accelerated Reliability Engineering. Colorado, United States: Hobbs Engineering Corporation
10. Hooper, J. H., and Amster, S. J. (1990), "Analysis and presentation of reliability data." Hand-book of Statistical Methods for Engineers and Scientists, edited by H. M. Wadsworth, New York: McGraw Hill.
11. Jensen F and Petersen N.E, "Burn-in, an engineering approach to the design and analysis of burn-in procedures", Wiley and sons, 1982
12. Jensen F, "Activation energies and the Arrhenius equation", Quality and Reliability Engineering International, Vol.1, No.1, p13-17, 1985
13. Johnston, D. R., LaForte, J. T., Podhorez, P. E., and Galpern, H. N. (1979), "Frequency acceleration of voltage endurance," IEEE Transaction on Electrical Insulation, HI-14, 121–126.
14. Joyce, W. B., Liou, K-Y., Nash, F. R., Bossard, P. R., and Hartman, R. L. (1985), "Methodology of accelerated aging" AT&T Technical Journal, 64, 717–764.
15. Klinger, D. J., Nakada, Y., and Menendez, M. A. (1990), AT&T Reliability Manual, New York: Van Nostrand Reinhold.
16. Meeker, W. Q. and Hahn, G. J. (1977), "Asymptotically Optimum Over-Stress Tests to Estimate the Survival Probability at a Condition with a Low Expected Failure Probability" (with discussion), Technometrics, 19, 381–399.
17. Meeker, W. Q., and Hahn, G. J. (1985), How to Plan an Accelerated Life Test-Some Practical Guidelines Volume 10 of the ASQC Basic References in Quality Control: Statistical Techniques. Available from the American Society for Quality Control, 310 W. Wisconsin Ave., Milwaukee, WI 53203.

18. Meeker, William Q., and Escobar, Luis A., *Statistical Methods for Reliability Data*, John Wiley & Sons, Inc., New York, 1998.
19. Meeker, W. Q., Escobar, L. A. and Lu, C. J. (1998), "Accelerated Degradation Tests: Modeling and Analysis," Technometrics 40, 89-99.
20. Meeker, W. Q., and Escobar, L. A. (1998), Statistical Methods for Reliability Data, New York: John Wiley & Sons.
21. MIL-HDBK-217F, "Reliability prediction of electronic components" Rome Laboratory, AFSC, Griffiss AFB, NY 13441-5700, 1986
22. Naikan, V.N.A., Reliability Engineering and Life Testing, PHI, New Delhi, 2010
23. Nelson Wayne, "Analysis of accelerated life test data-least square methods for the inverse power law", IEEE Transactions on Reliability, Vol.24, No.2, p103-107, 1975
24. Nelson Wayne, "Analysis of performance degradation data from accelerated life tests", IEEE Transactions on Reliability, R-30, N0.2, p149-155, 1981
25. Nelson, Wayne, *Accelerated Testing: Statistical Models, Test Plans and Data Analyses*, John Wiley & Sons, Inc., New York, 1990
26. O'Connor P.D.T, "Arrhenius and electronic reliability (Editorial)", Quality and Reliability Engineering International, Vol.5, 255, 1989.
27. Peck, D. S., and Zierdt, C. H. Jr. (1974), "The reliability of semiconductor devices in the Bell System" Proceedings of the IEEE, 62, 185–211.
28. Peck, D. S. (1986), "Comprehensive model for humidity testing correlation," Proceedings of the IEEE International Reliability Physics Symposium, 24, 44–50.
29. Smith, J. S. (1996), "Physics of failure." Handbook of Reliability Engineering and Management (Second Edition), Chapter 14, edited by W. G. Ireson, C. F. Coombs, and R. Y. Moss, New York: McGraw Hill.
30. Tobias, P. A., and Trindade, D. C. (1995), Applied Reliability (Second Edition), New York: Van Nostrand Reinhold.

Life Cycle Reliability and Safety Engineering
Vol.4 Issue 3 (2015) 36-46

Modified FMEA Model with Repair Effectiveness Factor using Generalized Renewal Process

Rajiv N Rai and Nomesh Bolia
Department of Mechanical Engineering, Indian institute of Technology Delhi, India
E-mail: rnrai08@gmail.com

Abstract

Conventional FMEA estimates Risk Priority Number (RPN) as a product of Severity (S), Probability of Occurrence (O) and Detection (D). In the existing practice of carrying out the usual FMEA, efforts to reduce RPN are done mainly by incorporating detection measures. Reducing (O) requires advanced reliability improvement measures like design modifications, etc which are time consuming, expensive and affects the fleet availability. This paper discusses Generalized Renewal Process (GRP) for an aero engine as a repairable component and introduces Repair Effectiveness Index (REI) denoted by q, estimated through GRP, in the FMEA of the aero engine. Hence a methodology is developed to estimate initial RPN by using REI, and then to reduce RPN of the failure modes (FM) by reducing (O) with the help of REI estimated through GRP. The potential of the proposed FMEA model is evaluated through a numerical example and duly validated with the existing field conditions.

Keywords: Generalized renewal process, Failure modes and effects analysis, Repair effectiveness index (q), Probability of occurrence (O), Detection (D).

Notations

a	Scale parameter
ABAO	As Bad as Old
AGAN	As Good as New
b	Shape parameter
D	Detection
FMs	Failure Modes
FMEA	Failure Modes and Effects Analysis
GRP	Generalized Renewal Process
MLEs	Maximum Likelihood Estimators
NHPP	Non- homogeneous Poisson process
O	Probability of Occurrence
OEM	Original Equipment Manufacturer
PRP	Perfect Renewal Process
RPN	Risk Priority Number
Q	Value of F (Vi | Vi-1) rated on a scale of 1-10 depending upon the range it falls.
REI (q)	Repair effectiveness index
S	Severity
t_{1OH}	Time to first overhaul of the aero engine
TBO	Time between Overhauls
v_n	Virtual age of the system after nth repair

1. Introduction

In general, an aero engine is exposed to imperfect repair on failing. An imperfect repair indicates that repair actions bring the state of a failed system to a level that is somewhere between new and that of prior to the failure. The concept of repairable systems, its applications, and the modeling of repairable systems with the help of Perfect Renewal

Process (PRP), Non Homogenous Process (NHPP) and Generalized Renewal Process (GRP) have been adequately discussed [1] – [3]. Research gaps in the field of imperfect repair with a focus on modeling repairable systems through GRP have been discussed in detail in [1] – [3]. This paper is aimed to develop Failure Mode Effect Analysis (FMEA) methods tailored for imperfect repairs. A brief literature survey of FMEA models modified for various settings is presented below.

Modified versions of FMEA have been developed by different researchers. Bowles and Pelaez [4] projects a method based on fuzzy logic for prioritization of failures for remedial actions in a Failure Mode Effects and Criticality Analysis (FMECA). Franceschini and Galetto [5] develop an exclusive methodology which can handle situations having diverse significance levels for the three FM component indices: severity, occurrence, and detection to decide the risk priority level (RPL) for the FMs. Sankar and Prabhu [6] propose a modified FMEA approach by introducing a new Risk Priority Rank (RPR) technique that utilizes a ranking scale of 1 to 1000 to characterize the increasing risk

of severity (*S*), probability of occurrence (*O*) and detection (*D*) combinations to prioritize failures in a system FMEA for initiating corrective actions. A modified adaptation of FMEA known as Total Failure Mode Effects Analysis (TFMEA) is developed [7] to bring out failure prevention for achieving continuous quality improvements. Pillay and Wang [8] develop Evidential Reasoning (ER) using fuzzy rules base and grey relation theory to rank the risks of different FMs in order to overcome the drawbacks of the conventional FMEA approach. Rhee and Ishii [9] present the details of life-cost based FMEA that measures risk in terms of cost over the life cycle. Hosseini and Safaei [10] introduce Decision Making Trial and Evaluation Laboratory (DEMATEL) for reprioritization of FMs based on severity of consequence or weight. A modified FMEA model with reliability and cost based approach is proposed [11] to overcome the drawbacks of traditional FMEA. Fuzzy based utility theory and fuzzy membership functions are utilized [12] to gauge severity, occurrence and detection. Structure of hierarchy and interdependence of corrective action is evaluated [13] by Interpretive Structural Model (ISM). The weight of a corrective action is then estimated through the analytic network process (ANP). Finally Chen [13] combines the utility of corrective actions to make a decision on improvement priority order of FMEA using Utility Priority Number (UPN). Fuzzy Risk Priority Numbers (FRPNs) is used [14] to prioritize FMs and used fuzzy geometric means to weigh the fuzzy ratings for *O, S* and *D*.

An exhaustive literature search has not revealed models explicitly developed to use REI in FMEA Models. Most of the papers have devised measures to reduce RPN by incorporating various detection techniques and on condition monitoring techniques. Literature on FMEA [15]-[16] also reveals the efforts to reduce RPN by reducing probability of occurrence mainly through design modifications. All these techniques require additions and alterations to be carried out on the present system which would not only prove to be expensive but will also consume time. For all these techniques to be incorporated, the equipment is required to be sent to original equipment manufacturer (OEM) which entails lots of administrative hassles. REI (q) is a function of correct maintenance procedures (a_0) proper maintenance hygiene (a_1), correct tools, testers & and ground equipments (a_2), standard spare parts (a_3) and so on. This can be written as:

$$q = f(a_0, a_1, a_2, a_3, \dots, a_n) \quad (1)$$

REI can be improved by following correct maintenance procedures, creating proper maintenance hygiene, using correct tools, testers & and ground equipments, using standard spare parts and so on. Thus improving the REI for each failure mode would directly reduce the probability of *O* since *O* is a function of *q*. This in turn will reduce RPN. Reducing *O* hence RPN will definitely help in containing the failure mode which in turn would enhance the reliability and availability of the equipment. This only requires a correct mind set of the maintenance manager rather than involving any major design changes or advanced condition monitoring techniques.

The first objective is to carry out FMEA of identified dominant failure modes [3] and develop a new algorithm for estimating RPN by introducing (*q*). Further a sensitivity analysis of the (*q*) on (*O*) is carried out and the final RPN is estimated with the suggested algorithm. The work is validated by achieving potential improvement due to applying the corrective measures by improving *q* .

The paper is structured as follows: section 2 introduces the GRP, section 3 introduces the FMEA process, section 4 formulates the problem, section 5 presents results and analysis, and section 6 concludes the work.

2. Generalized Renewal Process

Various performance measures like reliability, availability, MTBF and intensity function associated with GRP and concepts related to the virtual age along with GRP MLEs have been discussed at length [1] – [3]. The same ideas form a part of the methodology of this paper; hence are being reproduced for ready reference in sections 2.1 & 2.2.

2.1. Virtual Age and Repair Effectiveness (Kijima Model I)

Kijima & Sumita [17] developed an imperfect repair model by using the notion of the virtual age (V_n) process of a repairable system. Parameter V_n represents the calculated age of the system immediately after the nth repair occurs. If $V_n = y$, then the system has a time to the $(n+1)^{th}$ failure, X_{n+1}, which is distributed according to the following cdf:

$$F(x|v_n = y) = \frac{F(x+y) - F(y)}{1 - F(y)} \quad (2)$$

where F(x) is the cdf of the Time to first failure (TTFF) distribution of a new system or component. It is assumed that the n^{th} repair would only compensate for the damage accumulated during the time between the $(n-1)^{th}$ and the nth failure. With this assumption the virtual age of the system after the nth repair is:

$$V_n = V_{n-1} + qX_n \quad n=1, 2\ldots\ldots \tag{3}$$

where q is the repair effectiveness parameter, $V_0=0$. X_n is the time between the $(n-1)^{th}$ and the nth failure. If the times between the first and second failure (X_1) the second and third failure (X_2), $(i-1)^{th}$ and ith failure (X_i) etc, are considered, they can be expressed as

$$V_1 = qX_1$$

$$V_2 = q(X_1+X_2) \ldots V_n = q(X_1+X_2+\ldots\ldots+X_n)$$

$$V_n = q\sum_{i=1}^{n} X_i$$

$$V_i = q\sum_{j=1}^{i} X_j \tag{4}$$

where V_n and V_i are the virtual age at nth and i^{th} failures respectively. According to this model, when $q = 0$ the component is brought to 'as good as new' (AGAN) condition after the repair and thus can be modelled through PRP. Assumption of $q = 1$ signifies that the component is restored to the same condition which it was before the repair i.e. 'as bad as old'

(ABAO) condition which is modelled through NHPP. The values of q that fall in the interval $0 < q < 1$ represent the after repair state in which the condition of the system is better than old but worse than new. For $q > 1$, the system is in a condition of worse than old. Therefore q can be physically interpreted as an index for representing effectiveness and quality of repair.

2.2. Maximum Likelihood Estimators for GRP parameters

In this section it is intended to bring out equations used for deriving MLEs for the GRP performance parameters. Let t_i be the time between $(i-1)^{th}$ & i^{th} failure. Assuming a Weibull distribution for the inter failure times where a & b represents the scale & shape parameters respectively; following cdf & pdf can be derived [18]:

$$F(t_i) = 1 - \exp\left[a\left(q\sum_{j=1}^{i-1} t_j\right)^b - a\left(t_i + q\sum_{j=1}^{i-1} t_j\right)^b\right] \tag{5}$$

$$f(t_i) = ab[t_i + q\sum_{j=1}^{i-1} t_j)]^{b-1} \times \exp\left[a(q\sum_{j=1}^{i-1} t_j)^b - a\,(t_i + q\sum_{j=1}^{i-1} t_j)^b\right] \tag{6}$$

It is then possible to derive the MLEs for parameters *a*, *b* and *q* from the data, as shown in the next section.

2.2.1. Failure-terminated GRP MLEs

The likelihood function [18] is placed below at equation (7)

$$L = \left\{abt^{b-1}\exp\left[-at_1^b\right]\right\} \times \left\{\prod_{i=2}^{n}(ab)[t_i + q\sum_{j=1}^{i-1} t_j]^{b-1} \times \exp\begin{bmatrix} a\,(q\sum_{j=1}^{i-1} t_j)^b - \\ a\,(t_i + q\sum_{j=1}^{i-1} t_j)^b \end{bmatrix}\right\} \tag{7}$$

The logarithm of the likelihood function (equation 7) is differentiated with respect to each of the three parameters *a, b,* and *q* and after equating each derivative to zero, a system of three equations with three unknown variables [18] is obtained. For obtaining the values of *a, b* and *q* the equations (8, 9&10) shown below are required to be solved:

$$\frac{\partial[\ln(L)]}{\partial a} = \left(ba^{\frac{b+1}{b}}\right)\{\sum_{i=2}^{n}[\,(t_i + q\sum_{j=1}^{i-1} t_j)^b - (q\sum_{j=1}^{i-1} t_j)^b]\} + \left(ba^{\frac{1}{b}}\right)\left[at_1^b - n\right] = 0 \tag{8}$$

$$\frac{\partial[\ln(L)]}{\partial b} = \left[\frac{n}{b} + \ln(t_1) - n\ln\left(\frac{1}{a^{1/b}}\right) - at_1^b \ln\left(t_1 a^{\frac{1}{b}}\right)\right] + \sum_{i=2}^{n}[\ln\left(t_i + q\sum_{j=1}^{i-1} t_j\right) - a\,(t_i + q\sum_{j=1}^{i-1} t_j)^b \ln\left\{a^{\frac{1}{b}}(t_i + \sum_{j=1}^{i-1} t_j)\right\} + a\left(q\sum_{j=1}^{i-1} t_j\right)^b \ln\left\{\left(a^{\frac{1}{b}}\right)(q\sum_{j=1}^{i-1} t_j)\right\}\Big] = 0 \tag{9}$$

$$\frac{\partial[\ln(L)]}{\partial q} = (b-1) \times \{\sum_{i=2}^{n}\left(\frac{\sum_{j=1}^{i-1} t_j}{t_i + q\sum_{j=1}^{i-1} t_j}\right) + abq^{b-1} \sum_{i=2}^{n}(\sum_{j=1}^{i-1} t_j)^b - ab\sum_{i=2}^{n}[\,(t_i q\sum_{j=1}^{i-1} t_j)^{b-1}(\sum_{j=1}^{i-1} t_j)]\} = 0 \tag{10}$$

3. Failure Modes and Effects Analysis

FMEA [19] is performed by identifying the failure modes, finding out their causes and consequences, then estimating the probabilities of occurrence and finally determining corrective actions or preventive measures. It is generally performed as a bottom- up analysis, though it may be functional at any level in which there is adequate description to present the needed data. Distinctive steps [20] in conducting an FMEA include system definition, identification of failure modes, determination of cause, assessment

of effect, classification of severity evaluation of probability of occurrence and establishing corrective action. They are discussed as follows:

3.1. System Definition

The aim is to recognize those system components that are subject to failure. A functional and physical (hardware) description of the system provides the definition and margins for performing the analysis. Functional and physical descriptions are represented by flow diagrams depicting subassemblies, components, and parts along with their hierarchical interactions. With the help of these two diagrams, a reliability block diagram (RBD) is formed and used as the foundation for carrying out the analysis [19].

3.2. Identification of Failure Modes

Failure modes are known either by physical or functional failure. FMs display an evident behaviour in which a component fails. A few examples of FMs for an aero engine include damaged compressor blades, oil leak, engine overheat, damaged turbine blades, fuel leak, RPM fluctuation, excessive oil consumption, excessive vibration, etc [19]. Failure may also happen as an outcome of a premature incident, failure to function or become non operational at a given time, irregular operations or degraded performance.

3.3. Determination of Cause

A probable cause or causes [20] are bound to exist for each failure mode. Some specific examples of causes in case of aero engines are poor hydraulic discipline, environmental stress, poor maintenance practices, mechanical stress, fuel & oil contamination, fatigue, non –adherence to standard operating procedures, friction, temperature cycling, aging and wear out, substandard or defective parts, operator or maintenance induced error, corrosion, etc.

3.4. Assessment of Effect

Each failure has an impact on operations which affects the mission reliability and overall availability of the equipment. Effects may vary from total system failure to limited degradation on performance. System performances generally do not get affected immediately on failure of a redundant unit but it influences system reliability. Overall maintenance potential and system safety also gets affected [20].

3.5. Classification of Severity (S)

A range of severity classifications can be assigned to each failure mode for using as a basis for ranking remedial actions. Ebeling [19] classifies places failure in one of the following four categories.

Category I: Catastrophic. Significant system failure occurs that can result in injury, loss of life, or major damage.

Category II: Critical. Complete loss of system occurs. Performance is unacceptable.

Category III: Marginal. System is degraded, with partial loss in performance.

Category IV: Negligible. Minor failure occurs with no effect on acceptable system performance.

The basis of assigning numbers is subjective in nature and is based on the impact of the severity. Based on the failure, falling in one of the above four categories, it can be rated on a scale of 1 to 10. Category 1 can be rated as 10 whereas category IV can be rated as 1. The numbers assigned to categories III and IV will vary from 9-2 and will also vary from one individual to the other.

3.6. Estimation of Probability of Occurrence (O)

The probability of occurrence is based on the expected number of occurrences of each failure mode over a definite time period. This interval may be a mission time, a planned maintenance interval or the system design life. The following cdfs are used to estimate the probability of failure.

For the first failure [2]

$$F(v_1) = 1 - \exp\{-a(v_1)^b\} \quad (11)$$

For subsequent failures [2]

$$F(v_i|v_{i-1}) = 1 - \frac{R(v_i+v_{i-1})}{R(v_{i-1})} \quad (12)$$

$$F(v_i|v_{i-1}) = 1 - \exp a\left[(v_{i-1})^b - (v_i + v_{i-1})^b\right] \quad (13)$$

Ebeling [17] provides the following qualitative grouping of failure mode frequencies over the operating time interval.

Level A: Frequent. High probability of failure ($p \geq 0:20$)

Level B: Probable. Moderate probability of failure ($0.10 \leq p \leq 0.20$)

Level C: Occasional. Marginal probability of failure ($0.01 \leq p \leq 0.10$)

Level D: Remote. Unlikely probability of failure ($0.001 \leq p \leq 0.01$)

Level E: Extremely Unlikely. Rare event ($p < 0.001$)

Here again the basis of assigning numbers is subjective in nature and is based on the probability of failure. *O* is rated on a 10 point scale, e.g. Level A can be rated as 10 and level E as 1. Level B to D can be rated from 9-2 and this can vary from one individual to the other since it is subjective in nature.

3.7. Detection

Detection is the assessment of the likelihood that the mechanisms provided to prevent the cause of the failure mode from occurring will detect the cause of the FM or the failure mode itself. This is explained through an example. Sensors are provided as mechanisms in an aero engine to detect engine overheat. Hence, detection in this case is the assessment of likelihood that the sensors provided will detect engine overheat whenever it occurs. Detection is also described on a 10 point scale. Bad detection can be rated as 10 and good detection as 1.0 [20].

3.8. Computation of conventional RPN

This is a quantitative measure known as Risk priority Number for each failure mode that combines the probability of the failure modes occurrence with its severity ranking [20].

$$RPN = O*S*D \quad (14)$$

$$1 \leq RPN \leq 1000$$

3.9 Failure Mode Classification Matrix

A FMEA matrix is as shown in Figure 1.The cells contain the failure modes. In the vertical axis is the probability of occurrence and severity classification on the horizontal axis. As we move from the upper left corner of matrix to the lower right corner, the criticality and the severity of the failure mode become greater. The matrix then provides a guide to be used for eliminating and mitigating failures [20].

3.10. Determination of Corrective Action

Determination of corrective action depends on the failure modes and their RPN. More attention is required for the FMs having high RPN and severity classification. The corrective actions are initiated either to reduce *O*, *S* or improve *D*. This can be done by removing the cause of failure, decreasing probability of occurrence and reducing the severity of failure [20]. Decreasing (*O*) may require design modifications which are time consuming and costly as well. This will also have a direct impact on the availability of the fleet. This paper suggests corrective actions based on REI to reduce (*O*), which can improve RPN without resorting to any design changes/ modifications.

4. Problem Formulation

As mentioned in section 1, an aero engine has been selected as a case to develop the required methodology. The aero engines are subjected to general repairs on failing. They undergo periodic overhauls, OEM specified time between overhaul (TBO) being 550 hrs. Within an overhaul cycle, the aero engines also undergo OEM specified periodic maintenance at fixed intervals of 50 hrs. The OEM specified total technical life (TTL) of the aero engine is 1800 hrs. In this section we will firstly introduce various equations of the performance parameters to be estimated are firstly introduced and then RPN is evaluated through the proposed approach. Advantages of the proposed approach over the conventional method are also discussed.

4.1. Performance Parameters estimation

Let t_{1OH} be the time to the first overhaul and t_i denote the time of the i^{th} failure obtained from the failure data. With the help of field failure data for the first overhaul cycle, the initial aim is to estimate, a (scale parameter), b (shape parameter) and q (repair effectiveness factor) for the dominant failure modes of the aero engine. We compute the corresponding Intensity function, MTBF, Reliability, MTBF and availability using equations "equations (15) to (19)". All these parameters are required to be computed as they are measurable parameters through which we can detect the improvement in the performance of the aero engine after improving REI of each FM. The same is presented at table 9 subsequently. The Intensity function, MTBF, Reliability and Availability equations used in this paper have already been discussed in [2] and are reproduced below for better assimilation:

Intensity Function Equation

$$\lambda(v_i) = a \times b \times (v_i)^{b-1} \quad i=2, 3 \ldots n \quad (15)$$

Mean Time between Failures (MTBF) Equation

$$MTBF(v_i) = \frac{1}{\lambda(v_i)} \quad (16)$$

Reliability Equation

For first failure

$$R(v_1) = \exp\{-a(v_1)^b\} \quad (17)$$

For subsequent failures

$$R(v_i|v_{i-1}) = \frac{R(v_i+v_{i-1})}{R(v_{i-1})} = \exp a\left[(v_{i-1})^b - (v_i + v_{i-1})^b\right] \quad (18)$$

Availability Equation

$$A(v_i) = \frac{MTBF(v_i)}{MTBF(v_i)+MTTR} \quad i=2, 3....., n. \quad (19)$$

where MTTR stands for Mean Time to Repair.

4.2. The Proposed Approach

The conventional approach of estimating *O, S, D* and calculating RPN has been explained in detail in section 3. It is now aimed to develop the proposed algorithm based on REI *(q)*. The proposed approach is explained through a flow chart in Figure 2.

Substituting "Equation (4)" in "Equation (13)", following equation is obtained:

$$F(v_i|v_{i-1}) = 1 - \exp a\left[\left\{q\sum_{j=1}^{i-1} X_j\right\}^b - \left\{\left(q\sum_{j=1}^{i} X_j\right) + \left(q\sum_{j=1}^{i-1} X_j\right)\right\}^b\right] \quad (20)$$

From the above equation it can be seen that the failure probability $F(V_i \mid V_{i-1})$, and hence the probability of occurrence is directly related to *q*. It is recalled from equation (14) that the RPN is given by *O*S*D*. Here *O* is a measure of the probability of occurrence of the failures. The issue with using *O*, if the failure dynamics are governed by GRP is that it doesn't incorporate the effect of REI. In other words it is merely a measure of unconditional probability of occurrence, which is meaningful only for distribution where *q* is fixed to be 0 (renewal process) or 1(minimal repair). However, the only meaningful probability of occurrence for GRP is the conditional probability of occurrence, $F(V_i \mid V_{i-1})$. Therefore, the proposed approach works on replacing *O* with a measure of the conditional probability of occurrence (which is denoted by *Q*), thus incorporating the effect of *q*. *Q* can be obtained using the following steps:

(1) A curve is plotted between *q* Vs $F(V_i \mid V_{i-1})$.

(2) From equation (20) the corresponding values of F $(V_i \mid V_{i-1})$ for the estimated q from the failure data are obtained.

(3) The value of F $(V_i \mid V_{i-1})$ is rated on a scale of 1-10 depending upon the range it falls in as explained in section 3.6.

(4) *Q* is the value of the rating obtained in step 3.

Hence the proposed modified algorithm incorporating the effect of conditional probability of occurrence and REI for estimating RPN is placed below as equation (21):

$$RPN=Q*S*D \quad (21)$$

$$1 \le RPN \le 1000$$

The proposed algorithm is subjected to exhaustive analysis to check its efficacy and test it with the failure data of the aero engine in next section. The final RPNs for each failure mode are estimated after suggesting measures to improve *q*.

4.3. Advantage of Suggested Algorithm over Conventional Method

The conventional method of computation of RPN is discussed at section 3.8. It is comparatively more practical and economical to improve *q* and reduce

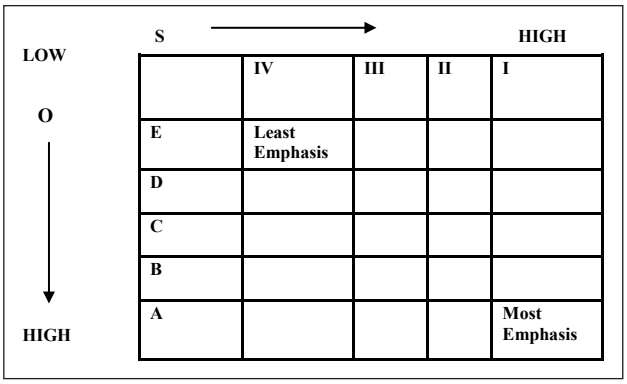

Figure 1. FMEA Matrix

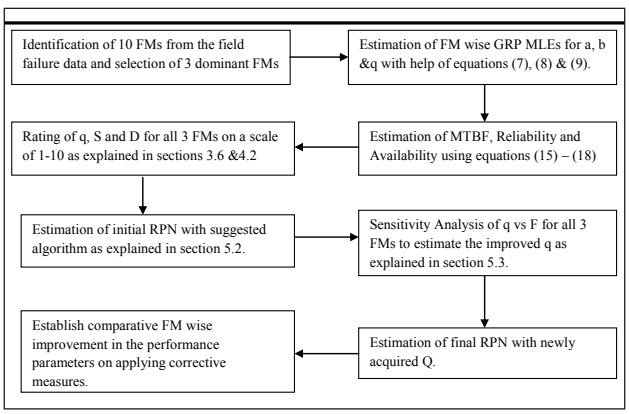

Figure 2. Flowchart of the proposed approach

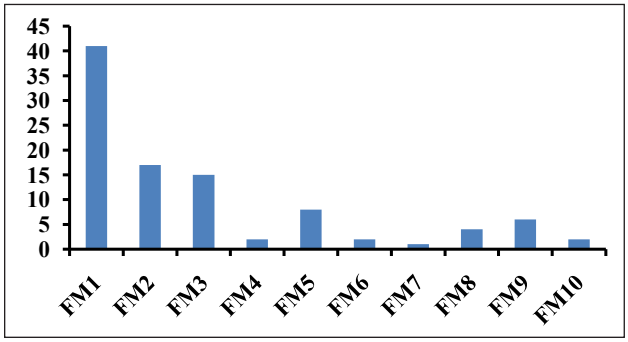

Figure 3. Categorization of Aero Engine FMs

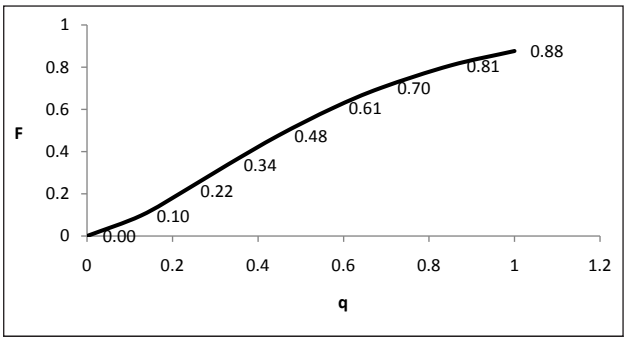

Figure 4. Sensitivity of q wrt F for FM1

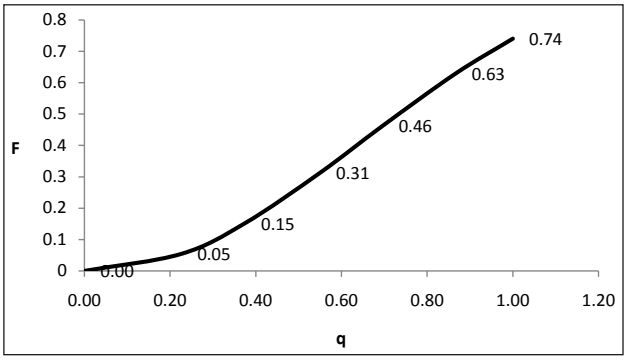

Figure 5. Sensitivity of q wrt F for FM2

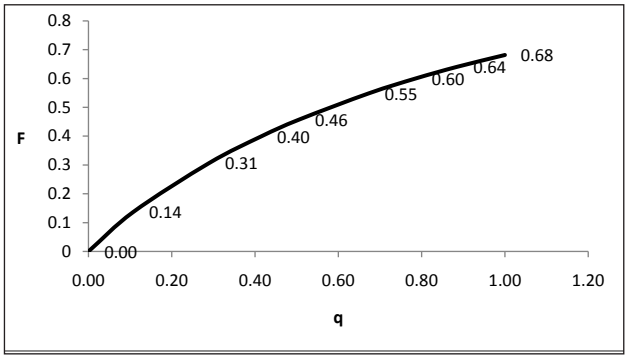

Figure 6. Sensitivity of q wrt F for FM3

RPN, rather than going for design modifications and improved/ additional condition monitoring techniques. REI is directly related to a number of maintenance functions as mentioned at equation (1) which can be addressed at the level of depot. Since improving *q* is in hands of the user itself, it will greatly help in improving the performance parameters over a short period of time without intervention of any external agencies and putting any extra burden to the exchequer.

5. Results & Discussion

The field failure data of 3 variants of the same aero engine for first overhaul cycle was collected and various FMs were worked out as discussed in section 5.1 followed by the procedure as explained in the flowchart placed at figure 2. In this section, the results of applied methodology to the selected aero engine are presented and discussed. The corrective actions are then discussed.

5.1. Estimation of GRP Estimators of the Identified Failure Modes

In Table 1, a list of 10 failure modes worked out from the failure data of the first overhaul cycle is presented. Selections of the FMs have been done from the failure data as per MIL-STD-1629A [20]. In our earlier paper [3] the same results for the failure modes and estimates for GRP were arrived at. Since the same results form a part of the methodology of this paper; hence they are reproduced for ready reference. The number of failures due to each mode has been plotted with the help of a line diagram and placed as Figure 3.The top three FMs are decided as dominant failure modes for the reason that number of failures due to more or less each of the remaining 7 FMs is less and that's why their contribution is inconsequential. Next, FM wise MLEs and performance parameters are estimated. The MLEs for values of *a, b, q* are then

Table 1. Failure Modes Identification

Number	Failure Mode	No of failures
FMI	Corrosion of compressor blades	41
FM2	Wear out of bearings	17
FM3	Creep-fatigue fracture of turbine blades	15
FM4	Fourth stage compressor disk crack	2
FM5	RPM Fluctuation	8
FM6	Crack on turbine blades	2
FM7	After burner diffuser crack	1
FM8	Engine not starting	4
FM9	High oil pressure	6
FM10	Excessive vibration	2

Table 2. Failure mode wise results for the first overhaul cycle

Failure	*a*	b	q	R(t=t_{1oh})	F(t=$_{1oh}$)	MTBF (t=t_{1oh})	A (t=t_{1oh})
Modes						(hrs)	
FM1	0.000153	1.46	0.85	0.1817	0.8183	261.96	0.3472
FM2	8.37*10^-7	2.14	2.7	0.0062	0.9938	206.92	0.3619
FM3	0.003644	0.92	1.0	0.3183	0.6817	494.16	0.5142

Table 3. Failure mode wise Initial RPN

Failure modes	*Q*	*S*	*D*	Initial RPN
				(Q*S*D)
FMI	10	10	8	800
FM2	10	8	1	80
FM3	8	10	2	160

Table 4. Failure mode wise values of final *Q*

Failure Modes	Estimated q	Initial Q	Improved q	Improved Q
FM1	**0.85**	**10**	**0.20**	**5**
FM2	**2.7**	**10**	**0.42**	**5**
FM3	**1.0**	**8**	**0.15**	**5**

Table 5. Final RPNs

Failure Modes	*Q*	*S*	*D*	Final RPN
FM1	5	10	8	400
FM2	5	8	1	40
FM3	5	10	2	100

Table 6. FM1

q	R(t=t_{1oh})	MTBF(t=t_{1oh})	A(t=t_{1oh})
0.85	0.1817	262 h	0.3472
0.20	0.8193	515h	0.5112
Percent Improvement	-	97	47

Table 7. FM2

q	R(t=t_{1oh})	MTBF(t=t_{1oh})	A(t=t_{1oh})
2.7	0.0062	207h	0.3619
0.42	0.8102	1128h	0.7556
Percent Improvement	-	-	109

Table 8. FM3 Table

q	R(t=t_{1oh})	MTBF(t=t_{1oh})	A(t=t_{1oh})
1.0	0.3183	494h	0.5142
0.15	0.8188	425h	0.4763
% Improvement	157	-	-

Table 9. Comparative results

q	R (t=t_{1oh})	MTBF (t=t_{1oh})	A (t=t_{1oh})
Before correction	0.00036	94h	0.0646
After correction	0.5435	193h	0.1840
Percent Improvement	-	105	185

obtained as explained in section 2.2. MTBF *(t=t_{1oh})*, *R (t=t_{1oh})*, & *A (t=t_{1oh})* are estimated using "Equations. (16) to (19)". In Table 2, the failure mode wise results for the aero engine for the first overhaul cycle are presented [3].

Various PMs for all the three FMs are presented to appreciate that if they were carried out as per laid down standard maintenance instructions, the failures could have been avoided and the number of failures against each FM would have decreased. This must have resulted in an improved REI (q). In case of compressor blades (FM1) if proper anti corrosive spray of proper specification is carried out during PM, corrosion can be prevented. Similarly if proper lubrication is carried out on concerned bearings with correct grade of oil, the effect and number of failures due to FM2 can be reduced. If Jet nozzles are properly serviced and electrical systems checked during PM, engine overheat can be avoided and failure of turbine blades (FM3) can be reduced.

Various repair processes undergone at repair facilities by the affected components against the three failure modes are also presented to appreciate the effectiveness of REI in improving the RPNs of these FMs. For FM1, the compressor blades have to go through the following processes [21]:

(1) Vibro grinding & Vibro tumbling

(2) Root sand blasting

(3) Root silver coating

For FM2 the only repair process is the replacement of bearings for which a number of components are required to be dissembled for the replacement. An engine test run is then given to ascertain the

serviceability. For FM3, the turbine blades undergo the following repair processes:

(1) Grinding of shroud platform
(2) Welding of blades
(3) Pre Final grinding
(4) Preliminary tool finish along the contour of overlaying and fillets.
(5) Heat treatment
(6) Final grinding
(7) Cleaning and finishing

5.2. Estimation of RPNS with suggested Algorithm

The next step is to rate repair effectiveness (q), severity (S) and detection (D) for all the three failure modes on a scale of 1-10 as explained in sections 3.6 & 4.2.

For FM1, since $F(t_{1oh}) = 0.8183$ which is greater than 0.20, the computed value of $q = 0.85$ can be rated as ($Q=10$). Since the compressor blade damage can lead to engine flame out in air, and may cause loss of both, the Pilot's life and aircraft, the severity can also be rated as 10. There is no cockpit indication for compressor blade damage but this can be checked only on ground, hence detection can be rated as 8.

In Case of FM2, $F(t_{1oh}) = 0.9938$ which is greater than 0.20, the computed value of $q= 2.7$ can be rated as ($Q= 10$). The oil leak can cause seizure of bearings and may lead to failure of engine lubrication system. Hence the consequences are quite severe, but since both visual and audio indications are provided, the aircraft can be landed under emergent conditions. Thus the severity (S) can be rated as 8 on a 10 point scale. The detection of oil leak can be done manually on ground and both visual and audio indications are provided in the cockpit, the detection is good both on ground as well as in the air. Hence detection (D) can be rated as 1 on 10 point scale.

For FM3, $F(t_{1oh}) = 0.6817$ which is again greater than 0.20 but comparatively lesser than the earlier two Failure modes and $q=1$, hence Q can be rated as 8 on a 10 point scale. The consequences of engine overheat could be disastrous and may lead to engine flame out in air leading to aircraft accident, loss of aircraft and loss of Pilot's life. Thus severity (S) can be rated as 10 on 10 point scale. Indications of both audio and visual have been provided in the cockpit, but there is no manual ways of checking engine overheat. Hence detection (D) can be rated as 2 on a 10 point scale.

In Table 3, the summary of failure mode wise of the values of Q, S, D obtained as discussed above are presented and then the values of initial RPN with the suggested methodology are estimated. It is observed from Table 3 that FM1 is the most serious failure mode having highest RPN followed by FM3 and FM2.

5.3. Corrective Actions

As discussed in Section 4.3, measures to reduce S or D are not suggested, since this involves suggesting design modifications etc. A sensitivity analysis between q and $F(V_i \mid V_{i-1})$ for all the failure modes are carried out to arrive at a value of improved q at which $F(V_i \mid V_{i-1})$ is brought below 0.20. Then the new RPNs are estimated followed by checking for improvement on all the performance parameters.

q vs. $F(V_i \mid V_{i-1})$ is plotted for FM1 in Figure 4 to highlight the sensitivity of q with respect to changes in F. From Figure 4 if the value of q is improved to 0.20 for FM1, then $F(V_i \mid V_{i-1}) = 0.185$ (hence less than 0.20), hence Q=5 is assigned. Similarly q Vs $F(V_i \mid V_{i-1})$ for FM2 is plotted in Figure 5 to highlight the sensitivity of q with respect to changes in F. For FM2, from Figure 5 the improved value of $q=0.42$ is obtained, then $F(V_i \mid V_{i-1}) = 0.19$ (hence less than 0.20) and $Q=5$ can be assigned. q vs. $F(V_i \mid V_{i-1})$ for FM3 is now plotted in Figure 6 to highlight the sensitivity of q with respect to changes in F. Lastly from Figure 6 if q is improved to 0.15 for FM3 then $F(V_i \mid V_{i-1})$ comes down to 0.1821(hence less than 0.20) and Q=5 can again be assigned.

In Table 4, the values of initial q and the improved q obtained through sensitivity analysis along with the rated value of q, i.e. Q are presented. In Table 5, the values of Final RPNs obtained with the value of newly acquired Qs are presented. It is observed from the Table 5, that RPNs have reduced by almost half on reducing the value of q, i.e. by improving the repair effectiveness without bringing out any changes in mitigating the consequences of failure or improving the detection techniques. In Tables 6, 7 & 8 the comparative Failure mode wise improvement in the performance parameters on applying corrective measures by improving the repair effectiveness q is presented.From Table 6 it is observed that the improvement observed in reliability is seemingly unrealistic and hence not reported. This is due to the extreme wear out and very poor maintenance during the first overhaul cycle as evident from the values of b & q respectively for FM1 from Table 2. Table 7 reveals

that the improvement observed in all the performance measures except availability is seemingly unrealistic and hence not reported. This is due to the extreme wear out and very poor maintenance during the first overhaul cycle as evident from very high values of *b* & *q* respectively. Due to very low values of reliability, MTBF and availability obtained during the first overhaul cycle, application of corrective measures in form of improving q from 2.7 to 0.42 has seen an upsurge in the improvement of reliability, MTBF & availability. From Table 8 it is noted that improvement in case of MTBF and Availability since value of *b* in case of FM3 is less than 1 may not be registered.

A significant improvement in all performance parameters by improving the repair effectiveness can be observed without actually resorting to adopting any drastic improvement measures. In Table 9, the comparative results of applying the corrective measures by improving the repair effectiveness (*q*), for the complete aero engine by combining the failure modes are presented. Since the failure modes are always in series *R (t),* MTBF (t), and *A (t)* is computed as

$$R(t)_{\text{aero engine}} = R(t)_{FM1} * R(t)_{FM2} * R(t)_{FM3} \quad (22)$$

$$A(t)_{\text{aero engine}} = A(t)_{FM1} * A(t)_{FM1} * A(t)_{FM1} \quad (23)$$

$$(t)_{\text{aero engine}} = (t)_{FM1} + (t)_{FM1} + (t)_{FM1} \quad (24)$$

$$\text{MTBF}(t)_{\text{aero engine}} = \frac{1}{\lambda(t)\text{aero engine}} \quad (25)$$

It is known from our experience that improving the repair quality results into the improvement in the repair effectiveness index (*q*) and leads to a significant improvement in reliability, MTBF and availability of the aero engines. The proposed methodology allows quantifying and hence planning the desired improvements. The improvement in case of reliability is seemingly unrealistic, hence not reported for the reasons that the rate of wear out

has been quite high and the quality of repair extremely poor during the first overhaul cycle, which is evident from the values of *b* and *q* for the first two failure modes. The potential ways and means of improving the REI have already been discussed in section 1.

6. Conclusion

Dominant failure modes of the aero engine were identified and then the performance parameters of the identified failure modes by treating the aero engines as a repairable system were estimated using GRP. This methodology not only provides shape and scale parameters but also renders an index to evaluate repair effectiveness. Conventional FMEA technique estimate RPN without incorporating repair effectiveness and suggest corrective measures to improve RPN by reducing *O*, *S* and increasing *D*. This can only be done through design changes or incorporating advanced condition monitoring techniques. This paper develops a methodology for estimating RPN by incorporating repair effectiveness into the conventional RPN algorithm. The paper presents the repair processes of the identified FMs for better appreciation of REI. The paper suggests ways for improvement of RPN by improving the repair effectiveness index *q* through adoption of measures like following correct maintenance procedures, creating proper maintenance hygiene, using correct tools, testers & and ground equipments, using standard spare parts and so on. REI can also be mathematically modelled as a function of all these factors (equation 1). A significant improvement in all the performance parameters such as reliability and availability can be seen by improving *q* rather than incorporating measures which involve design changes, sophisticated reliability improvement techniques and consequent high costs coupled with organizational resistance to big changes.

An extension to the work would be the application of multi criteria decision making (MCDM) techniques like AHP, ANP etc to all the factors mentioned at equation (1), based on the experience of concerned specialists in the field and the available data to obtain priority weights for them. Considering x_0, x_1, x_2, x_3… x_n be the priority weights attached to parameters , equation (1) can be written as:

$$q = (a_0x_0 + a_1x_1 + a_2x_2 + a_3x_3 +, \\ \ldots\ldots\ldots + a_nx_n) \quad (26)$$

where $0 \le q \le 1$, $0 \le a0 \le 1$, $0 \le a1 \le 1$, ……, $0 \le an \le 1$. The ranking of priority weights can be obtained using any of the standard MCDM techniques. With the help of simulation, the effect of each of these factors on REI and in turn on RPN of each FM can be examined for more precise results.

References

1. Bolia N., and Rai R.N., "Reliability based Methodologies for Optimal Maintenance Policies in Military Aviation", International Journal of Performability Engineering, Vol 9, pp.296-303, 2013.
2. Rai R.N., and Bolia N., "Availability based Methodologies

for Optimal Maintenance Policies in Military Aviation", Under Review at International Journal of Performability Engineering, 2013.

3. Rai R.N., and Bolia N., "Optimal Maintenance Policies in Military Aviation by identification of Dominant Failure Modes", Proceedings of the Institution of Mechanical Engineers, Part O: Journal of Risk and Reliability, Vol 228, No.1, pp.52-61, 2014.
4. Bowles J.B., and Peláez C. E., "Fuzzy logic prioritization of failures in a system failure mode, effects and criticality analysis", Journal of Reliability Engineering and System Safety, Vol 50, pp. 203-213, 2002.
5. Franceschini F., and Galetto M., "A New Approach for Evaluation of Risk Priorities of Failure Modes in FMEA", International Journal of Production Research, Vol 39, pp.2991-3002, 2001.
6. Sankar N.R., and Prabhu B. S., "Modified Approach for Prioritization of Failures in a System Failure Mode and Effects Analysis", International Journal of Quality and Reliability Management, Vol 18, pp. 324-335, 2001.
7. Devadasan S.R., Muthu R, Samson N, and Sankaran R.A., "Design of total failure mode and effects analysis programme", International Journal of Quality and Reliability Management, Vol 20, pp. 551-568, 2003.
8. Pillay A., and Wang J., "Modified failure mode and effects analysis using approximate reasoning", Journal of Reliability Engineering and System Safety, Vol 79,pp. 69-85, 2003.
9. Rhee S.J., and Ishii K., "Using Cost based FMEA to Enhance Reliability and Serviceability", Journal of Advanced Engineering Informatics, Vol 17, pp. 179-188, 2003.
10. Seyed-Hosseini S.M., Safaei N, and Asgharpour M.J., "Reprioritization of failures in a system failure mode and effects analysis by decision making trial and evaluation laboratory technique", Journal of Reliability Engineering and System Safety, Vol 91, pp. 872 – 881, 2005.
11. Arunachalam V.P., and Jegadheesan C., "Modified Failure Mode and effects Analysis, A Reliability and Cost-based Approach", The ICFAI Journal of Operations Management, Vol 5, pp. 7-20, 2006.
12. Dong C., "Failure mode and effects analysis based on fuzzy utility cost estimation", International Journal of Quality and Reliability Management, Vol 24, pp. 958 – 971, 2007.
13. Chen J. K., "Utility Priority Number Evaluation for FMEA", Journal of Failure Analysis and Prevention, Vol 7, pp. 321 – 328, 2007.
14. Wang Y.M., Chin K.S, Poon G.K and Yang J. B., "Risk evaluation in failure mode and effects analysis using fuzzy weighted geometric mean", Journal of Expert Systems with Applications, Vol 36 , pp. 1195-1207,2009.
15. Hoseynabadi-A,H., Oraee.H, and Tavner P.J., " Failure Modes and Effects Analysis (FMEA) for Wind Turbines", International Journal of Electrical Power &Energy Systems, Vol 32, pp.817-824,2010.
16. Bowles J.B., "An Assessment of RPN Prioritization in a failure Modes and Effects and Criticality Analysis", Annual Reliability and Maintainability Symposium, Florida, pp.380-386, 2003.
17. Kijima M., and Sumita U., "A useful generalization of Renewal Theory: counting process governed by non-negative Markovian increments", Journal of Applied Probability, Vol 23, pp. 71–88, 1986.
18. Yanez M., Joglar F, and Modarres M., "Generalized renewal process for analysis of repairable systems with limited failure experience", Reliability Engineering and System Safety, Vol 77, pp. 167–180, 2002.
19. Ebeling C. E., "An Introduction to Reliability and Maintainability Engineering", McGraw–Hill, 2007.
20. MIL-STD-1629 A. Procedures for performing a Failure Mode, Effects and Criticality Analysis, U.S Department of Defence 1980.
21. Rai R.N., and Bolia N., "Throughput Analysis of the Overhaul Line of a Repair Depot", Under Review at International Journal of Management Science and Engineering Management, 2014.

SRESA JOURNAL SUBSCRIPTION FORM

Subscriber Information (Individual)

Title	First Name	Middle Name	Last Name
_____	_____	_____	_____

Street Address Line 1	Street Address line 2
_____	_____

City	State/Province	Postal Code	Country
_____	_____	_____	_____

Work Phone	Home Phone	E-mail address
_____	_____	_____

Subscriber Information (Institution)

Name of Institution/ Library _____

Name and Designation of Authority for Correspondence _____

Address of the Institution/Library _____

Subscription Rates

	Subscription Quantity	Rate	Total
Annual Subscription (in India)	_____	Rs. 15, 000	_____
(Abroad)	_____	$ 500	_____
	_____		_____
	_____		_____

Payment mode (please mark)

Cheque ☐ Credit Card ☐ Master Card ☐ Visa ☐ Online Banking ☐ Cash ☐ De mand Draft ☐

Credit card Number _____

Credit Card Holders Name _____

Credit Card Holde _____

Guidelines for Preparing the Manuscript

A softcopy of the complete manuscript should be sent to the Chief-Editors by email at the address: editor@sresa.org.in. The manuscript should be prepared using 'Times New Roman' 12 font size in double spacing, on an A-4 size paper. The illustrations and tables should not be embedded in the text. Only the location of the illustrations and tables should be indicated in the text by giving the illustration / table number and caption.

The broad structure of the paper should be as follows: a) Title of the paper – preferably crisp and such that it can be accommodated in one or maximum two lines with font size of 14 b) Name and affiliation of the author(s), an abstract of the paper in ~ 100 words giving brief overview of the paper and d) Five key words which indicates broad subject category of the paper. The second page of the paper should start with the title followed by the Introduction

A complete postal address should be given for all the authors along with their email addresses. By default the first author will be assumed to be the corresponding author. However, if the first author is not the corresponding author it will be indicated specifically by putting a star superscript at the end of surname of the author.

The authors should note that the final manuscript will be having double column formatting, hence, the size of the illustration, mathematical equations and figures should be prepared accordingly.

All the figures and tables should be supplied in separate files along with the manuscript giving the figure / table captions. The figure and table should be legible and should have minimum formatting. The text used in the figures and tables should be such that after 30% reduction also it should be legible and should not reduced to less than font 9.

Last section of the paper should be on list of references. The reference should be quoted in the text using square bracket like '[1]' in a chronological order. The reference style should be as follow:

1. Pecht M., Das D, and Varde P.V., "Physics-of-Failure Method for Reliability Prediction of Electronic Components", Reliability Engineering and System Safety, Vol 35, No. 2, pp. 232- 234, 2011.

After submitting the manuscript, it is expected that reviews will take about three months; hence, no communication is necessary to check the status of the manuscript during this period. Once, the review work is completed, comments, will be communicated to the author.

After receipt of the revised manuscript the author will be communicated of the final decision regarding final acceptance. For the accepted manuscript the author will be required to fill the copy right form. The copy right form and other support documents can be down loaded from the SRESA website: http://www.sresa.org.in

Authors interested in submitting the manuscript for publication in the journal may send their manuscripts to the following address:

Society for Reliability and Safety
RN 68, Dhruva Complex
Bhabha Atomic Research Centre,
Mumbai – 400 085 (India)
e-mail : editor@sresa.org.in

The Journal is published on quarterly basis, i.e. Four Issues per annum. Annual Institutional Subscription Rate for SAARC countries is Indian Rupees Ten Thousand (Rs. 10,000/-) inclusive of all taxes. Price includes postage and insurance and subject to change without notice. For All other countries the annual subscription rate is US dollar 500 ($500). This includes all taxes, insurance and postage.

Subscription Request can be sent to SRESA Secretariat (please visit the SRESA website for details)

SRESA's International Journal of

Life Cycle Reliability and Safety Engineering

Contents

Vol.4 **Issue No.3** **July-Sep 2015** **ISSN – 2250 0820**